Rovibrational Energy Transfer in the $4\nu_{CH}$ Manifold of Acetylene, Viewed by IR−UV Double Resonance Spectroscopy. 5. Detailed Kinetic Model†

Mark A. Payne, Angela P. Milce, Michael J. Frost, and Brian J. Orr*

Centre for Lasers and Applications, Macquarie University, Sydney, NSW 2109, Australia

Received: August 23, 2007; In Final Form: October 13, 2007

Time-resolved infrared-ultraviolet double resonance (IR−UV DR) spectroscopy provides a distinctive way to examine collision-induced state-to-state energy transfer between rotational *J*-levels in vibrational manifolds of small polyatomic molecules, such as acetylene (C_2H_2) in its electronic ground state $\tilde{X}$. We consider the $4\nu_{CH}$ rovibrational manifold of C_2H_2 at ∼12 700 cm^{-1}, where the principal source of IR-brightness is the $(\nu_1 + 3\nu_3)$ or $(1\ 0\ 3\ 0\ 0)^0\ \Sigma_u^+$ vibrational combination level. In this highly congested manifold, anharmonic, *l*-resonance, and Coriolis couplings affect the *J*-levels of interest, implicating them in a complicated variety of intramolecular dynamics. Previous papers of this series have reported several seemingly anomalous *J*-resolved phenomena induced by collisions in C_2H_2 gas at room temperature with pressures and IR−UV pump−probe delay intervals corresponding to remarkably high Lennard-Jones collisional efficiencies $\mathscr{P}$: odd-Δ*J* rotational energy transfer ($10^{-3} < \mathscr{P} < 0.1$), in addition to regular even-Δ*J* transfer ($\mathscr{P} \approx 0.3$ for typical $|\Delta J| = 2$ transfer); particular rovibrational "gateway" channels, such as *via* $(\nu_1 + 3\nu_3)\ \Sigma_u^+\ J = 12$ (with $\mathscr{P}$ as high as ∼0.1); an apparently ubiquitous collision-induced quasi-continuous background ($10^{-3} < \mathscr{P} < 0.1$) that accounts for much of the observed collision-induced odd-Δ*J* satellite structure. These phenomena have been characterized by means of systematic IR−UV DR kinetic measurements, with IR pump and UV probe wavelengths and sample pressure fixed while the IR−UV pump−probe delay is scanned. In this paper, a detailed master-equation model is constructed to provide a satisfactory phenomenological fit to the IR−UV DR kinetic data, thereby offering mechanistic insight. This model includes collision-induced energy transfer between discrete rovibrational levels in an IR-bright manifold ***V*** and a quasi-continuous bath ***B***, mediated by a *J*-specific gateway manifold ***G***.

I. Introduction

There are numerous instances in molecular physics of significant scientific discoveries being preceded by courageous engineering projects that entail the building of new, high-performance instruments, taking advantage of emerging technology and almost invariably driven by a visionary determination to make measurements that surpass what were previously feasible. A prime example in this context is the emergence of optothermal molecular-beam spectroscopy, pioneered 30 years ago by Gough, Miller, and Scoles.[1,2] Several key technological elements were involved in this development: a liquid-helium-cooled doped silicon superconducting bolometer[2,3] which operated at ∼2 K and was of a type previously used to measure molecular beam scattering;[4] continuous-wave single-longitudinal-mode F-center lasers[2,5] that were continuously tunable in the near-infrared region, with new-found reliability; a profound insight into high-vacuum technology, enabling essential instrumental engineering to be optimized.[2,6−8] (In this last respect, Scoles[9] has lauded "the superiority of common sense over complicated thinking," as exemplified in J. B. Fenn's approach to such research.)

Among the myriad scientific outcomes of optothermal spectroscopy are the following areas in which significant, topically relevant advances have been made: structure and dynamics (e.g., infrared predissociation) of complexes and clusters of molecules;[1,2,10,11] rotational and vibrational energy transfer;[12−14] differential scattering;[15] high-field laser Stark spectroscopy of nondipolar molecules;[16−18] photofragmentation of oriented complexes;[14,19−21] eigenstate-resolved infrared spectroscopy of congested polyatomic-molecular rovibrational manifolds;[22−26] scattering of atoms[27,28] or molecules[29] from surfaces; superfluid-helium nanodroplet spectroscopy.[30−34]

Topics such as these have recently been reviewed[35] in the context of the spectroscopy and energetics of the molecule that is central to the present paper, namely, acetylene (C_2H_2), for which some relevant spectroscopic nomenclature[35,36] is summarized in Table 1. Indeed, our ongoing interest[37−42] in the $4\nu_{CH}$ rovibrational manifold of C_2H_2 (at ∼12 700 cm^{-1} in its $\tilde{X}^1\Sigma_g^+$ electronic ground state) was first stimulated[37] by the laser Stark spectra of C_2H_2, optothermally detected in a molecular beam by Gough and co-workers.[17] Moreover, our preceding studies[43−46] of the $(\nu_{CC} + 3\nu_{CH})$ region at ∼11 600 cm^{-1} in the $\tilde{X}$ manifold of C_2H_2 have reciprocally prompted optothermal laser Stark spectroscopy in that same region[18] and have facilitated interpretation[46] of the complexities encountered there.

The principal technique employed in our experiments on C_2H_2 is time-resolved infrared-ultraviolet double resonance (IR−UV DR) spectroscopy, with detection by laser-induced fluorescence (LIF).[35,37−46] The IR−UV DR excitation scheme illustrated in Figure 1 depicts the way that collision-induced rovibrational energy transfer (ET) can be distinguished by varying the IR−UV delay, *t*, between rotationally selective IR pump and UV

† Part of the "Giacinto Scoles Festschrift".

* To whom correspondence should be addressed. E-mail: borr@ics.mq.edu.au.

10.1021/jp0767617 CCC: $37.00
Published on Web 12/06/2007

TABLE 1: Summary of Spectroscopic Notation Applicable to $^{12}C_2H_2$ in the Context of This Paper[a]

spectroscopic property	notation and characteristics
term symbols for electronic states[b]	$\tilde{X}\ ^1\Sigma_g^+$ ($T_e = 0$ cm^{-1}; $D_{\infty h}$); $\tilde{A}\ ^1A_u$ ($T_e = 42\,197.57$ cm^{-1}; C_{2h})
normal modes of vibration, $i = 1-5$ (for $\tilde{X}\ ^1\Sigma_g^+$ electronic ground state)[c]	$i = 1$: symmetric CH stretch, ν_1 (σ_g^+; $G_v = 3\,372.85$ cm^{-1}); $i = 2$: CC stretch, ν_2 (σ_g^+; $G_v = 1\,974.32$ cm^{-1}); $i = 3$: antisymmetric CH stretch, ν_3 (σ_u^+; $G_v = 3294.84$ cm^{-1}); $i = 4$: symmetric *trans*-CCH bend, ν_4 (π_g; $G_v = 612.87$ cm^{-1}); $i = 5$: antisymmetric *cis*-CCH bend, ν_5 (π_u; $G_v = 730.33$ cm^{-1})
vibrational angular momenta, l_i and l (for $\tilde{X}\ ^1\Sigma_g^+$ electronic ground state)[d]	$i = 4$: l_4; $i = 5$: l_5; resultant: $l = l_4 + l_5 \equiv k$ (associated with doubly degenerate bending modes ν_4 and ν_5)
zero-order normal-mode basis states[e]	$\lvert(V_1\ V_2\ V_3\ V_4^{l_4}\ V_5^{l_5})^l_\pm\rangle$, where the $\pm$ label applies to $l = 0$ levels
anharmonically coupled vibrational polyad states[f]	$\lvert\{n_s, n_{res}, l, g/u, \pm\}\rangle$, where $n_s = V_1 + V_2 + V_3$; $l = l_4 + l_5$; (for C_2H_2) $n_{res} = 5V_1 + 3V_2 + 5V_3 + V_4 + V_5$ (V_1, V_2, V_3, V_4, l_4, V_5, l_5 are spoiled as good quantum numbers)
polyad states coupled by off-diagonal l-resonance[g]	$\lvert\{n_s, n_{res}, g/u, \pm\}\rangle$, so that l is also spoiled as a good quantum number and the resulting levels are no longer pure Σ, Π, Δ, ...
coriolis-coupled vibrational polyad states[h]	$\lvert\{n_{res}, g/u, \pm\}\rangle$, where V_1, V_2, V_3, V_4, l_4, V_5, l_5, l, and n_s are all spoiled as good quantum numbers
specific rovibrational manifolds[i]	$4\nu_{CH}$ at $\sim$12 700 cm^{-1}, based on ($\nu_1 + 3\nu_3$), i.e., $(1\ 0\ 3\ 0\ 0)^0$; ($\nu_{CC} + 3\nu_{CH}$) at $\sim$11 600 cm^{-1}, based on ($\nu_2 + 3\nu_3$), i.e., $(0\ 1\ 3\ 0\ 0)^0$

[a] This tabular summary, based on refs 35 and 36, defines electronic states, normal modes of vibration, vibrational quantum numbers, and vibrational eigenstates (in the presence of various classes of intramolecular perturbation) for $^{12}C_2H_2$ that are of particular relevance to this paper. [b] Term symbols and term energies T_e for the lower and upper electronic states of $^{12}C_2H_2$ implicated in our IR−UV DR experiments. [c] Normal-mode vibrational labels, ν_i ($i = 1-5$), for the $\tilde{X}^1\Sigma_g^+$ electronic ground state of $^{12}C_2H_2$, together with corresponding symmetry species and vibrational term energies G_v. [d] Vibrational angular momentum quantum numbers, l_i ($i = 4, 5$), and their resultant $l = l_4 + l_5$ (also designated as k in some of the literature) associated with doubly degenerate bending modes in the $\tilde{X}^1\Sigma_g^+$ electronic ground state of C_2H_2; $l = 0, 1, 2, 3, \ldots$ levels have Σ, Π, Δ, Φ, ... labels, respectively. [e] Zero-order basis states for vibrational levels in the $\tilde{X}^1\Sigma_g^+$ electronic ground state of C_2H_2, labeled in terms of normal-mode quantum numbers, V_i ($i = 1 - 5$), l_4, l_5, l, and a $\pm$ symmetry label that is also necessary when $l_4 = -l_5$ (i.e., $l = 0$) and which corresponds to Σ^+/Σ^- states. [f] Vibrational polyad (or cluster) description for $\tilde{X}^1\Sigma_g^+$ C_2H_2, in the presence of anharmonic coupling. [g] Polyad description in the presence of off-diagonal l-resonance coupling, where l is not well-defined. [h] Coriolis-coupled vibrational polyad description, in which only the polyad label n_{res}, the point-group symmetry label g/u, and the $\pm$ symmetry label remain well-defined. [i] Qualitative labels and frequencies for the rovibrational manifolds that have been studied in our IR−UV DR experiments (see refs 37−46), together with their principal source of IR brightness.

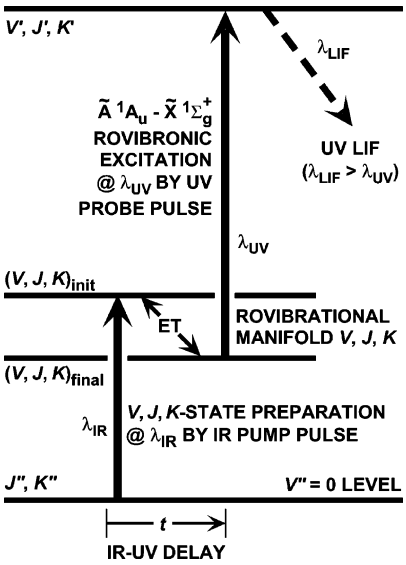

Figure 1. Excitation scheme for time-resolved, LIF-detected IR−UV DR spectroscopy of C_2H_2. Discrete rovibrational levels $(V, J, K)_{init}$ and $(V, J, K)_{final}$ in the manifold of interest are coupled by collision-induced energy transfer (ET) during the IR−UV delay interval t.

probe pulses. This provides a distinctive way to examine collision-induced state-to-state energy transfer between rotational J-levels in vibrational manifolds of small polyatomic molecules, such as C_2H_2. LIF-detected IR−UV DR spectroscopy is another example of scientific advances being driven by new enabling technology (in this case, nanosecond-pulsed Nd:YAG lasers and associated continuously tunable sources of narrowband coherent radiation).

IR−UV DR spectroscopy of rovibrational energy transfer in the ν_{CH} manifold of C_2H_2, centered at $\sim$3288 cm^{-1}, has been studied extensively by Smith, Frost, and co-workers.[47−52] In particular, Frost's early UV-scanned, LIF-detected IR−UV DR experiments[48] have yielded insight into ways in which intramolecular perturbations, such as anharmonic coupling in the ($\nu_3/\nu_2 + \nu_4 + \nu_5$) Fermi-type dyad of C_2H_2, can influence rotationally resolved propensities and cross sections for collision-induced intramolecular $V-V$ transfer between the $(\nu_3/\nu_2 + \nu_4 + \nu_5)_I$ and $(\nu_3/\nu_2 + \nu_4 + \nu_5)_{II}$ submanifolds.[35,53,54]

CH-stretching overtone and combination bands above $\sim$6500 cm^{-1} in the near-IR absorption spectrum of C_2H_2 entail excitation to congested assemblies of rovibrational levels, many of which are strongly perturbed relative to basis states from which they are derived. Crim and co-workers[55−63] are the principal pioneers of LIF-detected IR−UV DR spectroscopy with near-IR pump excitation in the $\tilde{X}$ manifold above $\sim$6500 cm^{-1}. Absorption spectra in the $n_s\nu_{CH}$ ($n_s = 2-5$) regions of C_2H_2 correspond to excitation of n_s CH stretching quanta (ν_1 and/or ν_3), where n_s is a polyad quantum number as defined in Table 1. The upper vibrational IR absorption levels that carry the oscillator strength in the $n_s\nu_{CH}$ rovibrational manifolds of C_2H_2 are as follows:[35,36,64,65] for $n_s = 2$, $(\nu_1 + \nu_3)$ at $G_v = 6556.46$ cm^{-1}, primarily $(1\ 0\ 1\ 0^0\ 0^0)^0_+$; for $n_s = 3$, $3\nu_3$ at $G_v = 9639.85$ cm^{-1}, primarily $(0\ 0\ 3\ 0^0\ 0^0)^0_+$; for $n_s = 4$, $(\nu_1 + 3\nu_3)$ at $G_v = 12\,675.68$ cm^{-1}, primarily $(1\ 0\ 3\ 0^0\ 0^0)^0_+$; for $n_s = 5$, $5\nu_3$ at $G_v = 15\,948.52$ cm^{-1}, primarily $(0\ 0\ 5\ 0^0\ 0^0)^0_+$. To first order (i.e., in the absence of local off-diagonal l-resonance or Coriolis perturbations), all of these levels have Σ_u^+ vibrational symmetry with well-defined l (=0) and point-group symmetry (+).[35,36] Crim and co-workers have addressed various key issues

TABLE 2: Index to IR−UV DR Studies of the $4\nu_{CH}$ Manifold in C_2H_2 by Payne, Milce, and co-workers[a]

ref (year)	topic	content/significance
37 (1997)	dynamical symmetry breaking (?) in $4\nu_{CH}$[b]	our initial results, prompted by ref 17 and showing ET gateway anomalies in the $(\nu_1 + 3\nu_3)\ \Sigma_u^+$ $J = 1$ and $J = 12$ levels
38 (2000)	quasi-continuum of background states	first evidence of a collision-induced quasi-continuous background (CIQCB) that is ubiquitous in $4\nu_{CH}$ IR−UV DR spectra
46 (2000)	$(\nu_{CC} + 3\nu_{CH})$ rovibrational manifold ...	detailed analysis of intramolecular perturbations; contrasting collision-induced ET mechanisms in $(\nu_{CC} + 3\nu_{CH})$ and $4\nu_{CH}$
66 (2000)	applications of optical parametric oscillators	IR pump and UV probe sources with narrower optical bandwidths fail to reveal any new underlying IR−UV DR effects.
39 (2003)	1. foundation studies at low J[c]	systematic IR−UV DR characterization of $(\nu_1 + 3\nu_3)\ \Sigma_u^+$ $J = 0$ and $J = 1$ rovibrational levels, refining results of ref 37
40 (2005)	2. perturbed states with $J = 17$ and 18[c]	systematic IR−UV DR characterization of $4\nu_{CH}$ $J = 17$ and $J = 18$ rovibrational levels, affected by strong local perturbations
41 (2005)	3. state-to-state J-resolved kinetics[c]	procedures needed to preprocess IR−UV DR kinetic data; preliminary report of a rate-equation model and its results
42 (2006)	4. collision-induced quasi-continuous background effects[c]	detailed IR−UV DR spectroscopy and kinetics to characterize the CIQCB effect and its proposed mechanism (involving collisional ET to a congested IR-dark rovibrational manifold)
this work	5. detailed kinetic model[c]	details of a phenomenological master-equation model to fit IR−UV DR kinetics in the $4\nu_{CH}$ manifold (including CIQCB)

[a] This general subject area has recently been reviewed in ref 35. [b] The proposition that genuine collision-free "dynamical symmetry breaking" occurs in the $4\nu_{CH}$ manifold of C_2H_2 has subsequently been discredited (see refs 35, 38−42, and 46). [c] Subtitle of a part of this ongoing series of papers entitled "Rovibrational energy transfer in the $4\nu_{CH}$ manifold of acetylene, viewed by IR−UV double resonance spectroscopy," by Payne et al.

in the $\tilde{X}$ manifold of C_2H_2 at high vibrational energies (above 6500 cm^{-1}), including J-resolved state-to-field relaxation of the $n_s\nu_{CH}$ ($n_s = 2-4$) manifolds, *via* C_2H_2/C_2H_2 collisions and with rare-gas collision partners;[55,56,62] even-$|\Delta J|$ state-to-state rotational energy transfer (RET) within the $3\nu_{CH}$ manifold *via* collisions with C_2H_2[57,62] or Ar;[62] J-resolved state-to-state intrapolyad $V-V$ transfer within the $3\nu_{CH}$ manifold *via* C_2H_2/C_2H_2 collisions;[57,61] recognition of the complementary roles of IR-bright/UV-dark and IR-dark/UV-bright rovibrational states in IR−UV DR spectra of C_2H_2.[63] They have also assigned and characterized rovibronic structure in the $\tilde{A}^1A_u$ excited electronic state of C_2H_2, using reduced term-value plots[58,59] and normal-mode analysis.[60]

Continuing that line of investigation (and within the context of the present paper) we have made extensive IR−UV DR spectroscopic investigations of the $4\nu_{CH}$ manifold of C_2H_2 at ~12 700 cm^{-1}, as summarized in Table 2.[37−42,46,66] These interests stem from our IR−UV DR spectroscopic studies[43−46,46,66] of contrasting dynamical behavior in the adjacent $(\nu_{CC} + 3\nu_{CH})$ manifold, which draws its rovibrational oscillator strength from the $(\nu_2 + 3\nu_3)\ \Sigma_u^+$ basis state, i.e., $(0\ 1\ 3\ 0^0\ 0^0)_+^0$, with $G_v = 11\,599.68\ cm^{-1}$.

The investigations summarized in Table 2 are of particular interest in the present paper. In terms of the generic time-resolved IR−UV DR excitation scheme for C_2H_2 depicted in Figure 1, they involve intermediate rovibrational levels (V, J, K) of the $4\nu_{CH}$ manifold, for instance, from the IR-bright $(\nu_1 + 3\nu_3)\ \Sigma_u^+$ level with $G_v = 12\,675.68\ cm^{-1}$ and primary basis state $(1\ 0\ 3\ 0^0\ 0^0)_+^0$. A narrowband IR PUMP laser pulse tuned to transitions of form $(V, J, K)_{init} \leftarrow (V'' = 0, J'', K'')$ is used for selective excitation of C_2H_2 to rovibrational levels $(V, J, K)_{init}$ of the $4\nu_{CH}$ manifold. Rovibrational energy transfer (ET; marked by a double-headed arrow in Figure 1) within the $4\nu_{CH}$ manifold takes C_2H_2 molecules from the prepared level $(V, J, K)_{init}$ to a destination level $(V, J, K)_{final}$. This destination level is monitored by means of a pulsed tunable UV PROBE laser that excites rovibronic transitions $(V', J', K') \leftarrow (V, J, K)_{final}$ in the $\tilde{A}-\tilde{X}$ absorption system, with LIF detection from the $\tilde{A}\ ^1A_u$ electronic manifold.

Within this time-resolved, LIF-detected IR−UV DR approach, there are two distinct forms of sequential excitation. The former is direct, which is effectively free of intervening collision-induced energy transfer within the intermediate rovibrational manifold (V, J, K), as follows:

$$\text{Direct excitation: } (V', J', K') \leftarrow \text{UV} - (V, J, K) \leftarrow \text{IR} - (V'', J'', K'') \quad (1)$$

with $V'' = 0$, as depicted schematically in Figure 1, and $(V, J, K)_{init}$ and $(V, J, K)_{final}$ indistinguishable; the "←" arrows denote spectroscopic transitions (stimulated by IR PUMP or UV PROBE radiation). The other form of excitation is indirect, arising when values of t and P are sufficiently large to enable collision-induced state-to-state energy transfer (ET) during the IR−UV delay interval, as follows:

$$\text{Indirect transfer: } (V', J', K') \leftarrow \text{UV} - (V, J, K)_{final} \leftarrow \text{ET} - (V, J, K)_{init} \leftarrow \text{IR} - (V'', J'', K'') \quad (2)$$

where "← ET −" denotes collision-induced energy transfer (e.g., J-resolved $V-V$ transfer or RET). IR−UV DR spectra are often displayed as difference spectra, with the thermal-equilibrium background signal electronically suppressed to show only the IR PUMP-induced DR signal.

In our IR−UV DR experiments on C_2H_2 gas at sample pressure P, the ET processes of interest are induced by collisions during a controllable IR−UV delay interval t. As before,[37−46] the combination of P and t define the collision number z, referred arbitrarily to Lennard-Jones collisional rate constants k_{LJ}. (For C_2H_2/C_2H_2 self-collisions at 300 K, values of z are referred to $k_{LJ} = 16.4\ \mu s^{-1}\ Torr^{-1} = 5.10 \times 10^{-10}\ cm^3\ molecule^{-1}\ s^{-1}$.[62]) Continuous variation of t while systematically fixing the IR PUMP and UV PROBE wavelengths (λ_{IR} and λ_{UV}, respectively) at constant P yields sets of IR−UV DR kinetic curves, which comprise plots of self-consistent, internally calibrated IR−UV DR signal amplitude versus t.[37−42,45]

This paper describes a rate-equation model that is able to reproduce such IR−UV DR kinetic curves and thereby provide detailed phenomenological insight into the complicated network of underlying collision-induced rovibrational energy transfer (ET) processes that occur within the $4\nu_{CH}$ manifold of C_2H_2. These IR−UV DR kinetic curves are complemented by various

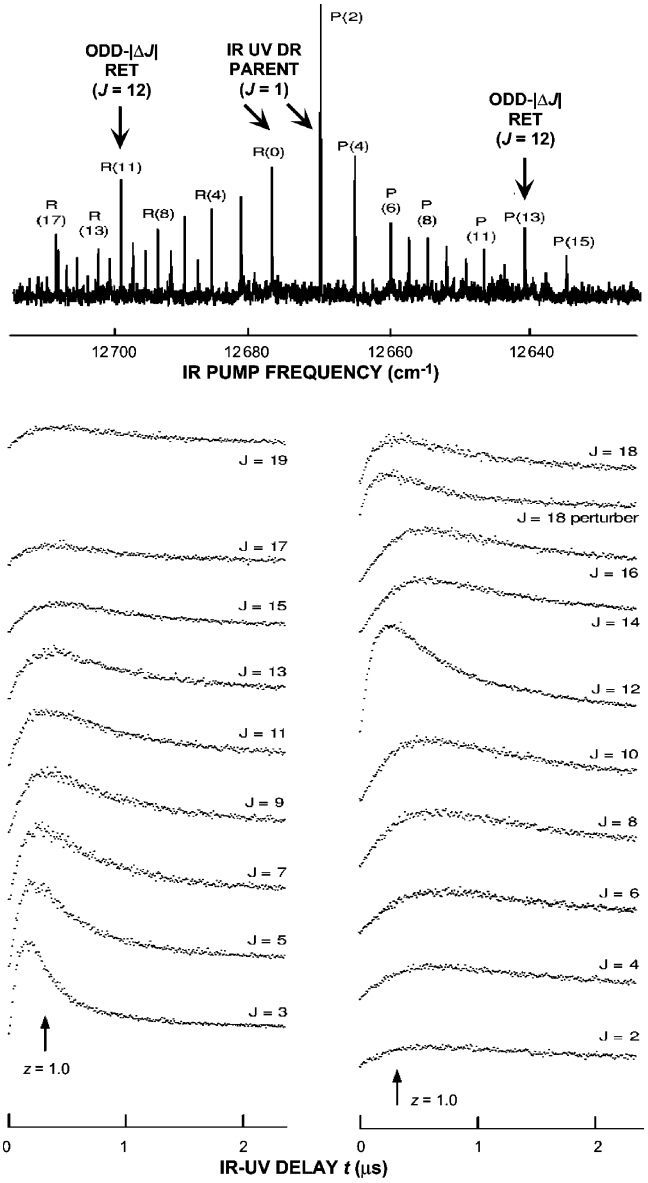

Figure 2. Time-resolved LIF-detected IR−UV DR spectroscopic results for C_2H_2 probed in the $(\nu_1 + 3\nu_3)\ \Sigma_u^+\ J_{final} = 1$ level:[37,39] upper, IR-scanned with $z = 0.66$; lower, kinetics for specific J_{init} levels. Calibrated in a self-consistent fashion to indicate actual relative IR−UV DR signal amplitudes.

IR-scanned IR−UV DR spectra (with λ_{IR} tuned while λ_{UV}, t, P, and z are fixed) and UV-scanned IR−UV DR spectra (with λ_{UV} tuned while λ_{IR}, t, P, and z are fixed), as reported in our earlier articles on the $4\nu_{CH}$ manifold of C_2H_2.[37−42,46,66]

II. A Specific Example: IR−UV DR Spectroscopy of C_2H_2 Probed in the $(\nu_1 + 3\nu_3)\ \Sigma_u^+\ J = 1$ Level

Figure 2 depicts time-resolved, LIF-detected IR−UV DR spectroscopic results (comprising portions of Figures 2 and 3 of ref 39), where the wavelength of the UV PROBE laser pulse is set at 299.105 nm, which unambiguously monitors the rovibrational destination level $(\nu_1 + 3\nu_3)\ \Sigma_u^+\ J_{final} = 1$ *via* the $R(1)$ rovibronic transition of C_2H_2 in its $\tilde{A}-\tilde{X}\ 1_1^0\ 3_3^1\ 5_0^1\ K_0^1$ absorption band.[37,39] The topmost portion of Figure 2 is an IR-scanned IR−UV DR spectrum that spans the 12 676 cm^{-1} $(\nu_1 + 3\nu_3)\ \Sigma_u^+ - \Sigma_g^+$ combination band of C_2H_2.[37−39] Collision-induced R- and P-branch features appear as the narrowband pulsed IR PUMP laser is tuned to successive $(V, J, K)_{init} \leftarrow$ $(V'' = 0, J'', K'')$ transitions, which communicate *via* collision-induced ET to the $(V, J, K)_{final}$ $J = 1$ level that is LIF-detected by the UV PROBE laser. Small values of z (e.g., $z = 0.033$, with $t = 10$ ns and $P = 0.20$ Torr); not explicitly depicted in Figure 2)[37−39] yield a simple two-line IR−UV DR spectrum comprising only the $R(0)$ and $P(2)$ rovibrational "parent" features (designated by diagonal arrows in Figure 2, at 12 677.98 and 12 670.92 cm^{-1}, respectively) owing to direct, collision-free excitation as in eq 1. A 20-fold increase in z (e.g., with $t = 200$ ns and $P = 0.20$ Torr, as in the topmost portion of Figure 2)[37,39] yields a more congested IR-scanned IR−UV DR spectrum, with a series of $R(J_{init} - 1)$ and $P(J_{init} + 1)$ rovibrational features corresponding to odd values of J_{init} in the $(\nu_1 + 3\nu_3)$ band of C_2H_2; this is consistent with the expected even-$|\Delta J|$ RET satellites *via* an indirect, collision-induced excitation scheme as in eq 2. The corresponding IR−UV DR kinetic curves[39] (recorded with $P = 0.20$ Torr and the IR PUMP tuned to successive odd-J_{init} peaks in the $(\nu_1 + 3\nu_3)$ band of C_2H_2) are shown in the lower left-hand column of Figure 2; an upward-pointing arrow designates the value of t at which $z = 1.0$.

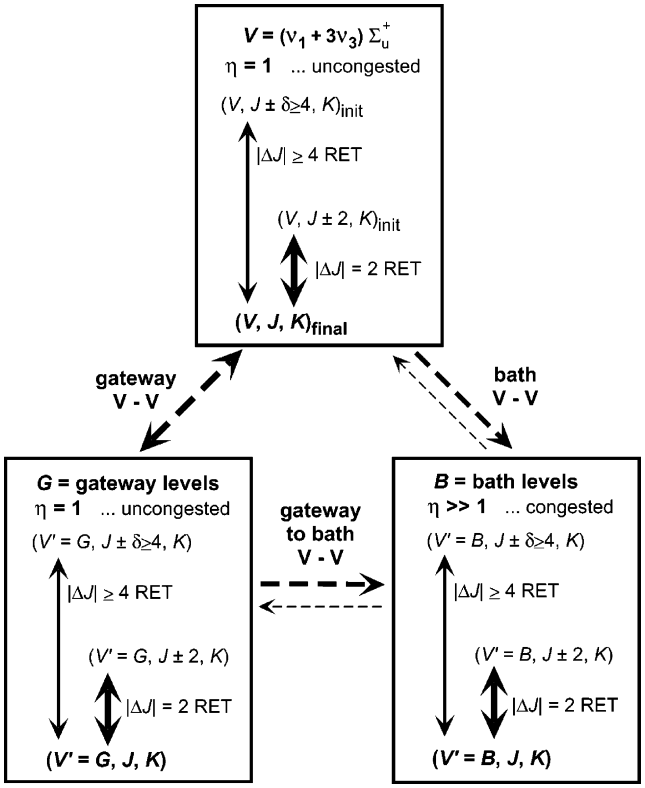

Figure 3. Schematic model of IR−UV DR kinetics in the $4\nu_{CH}$ manifold of C_2H_2, based on three distinct rovibrational submanifolds: ***V***, directly monitored $(\nu_1 + 3\nu_3)\ \Sigma_u^+$ levels; ***G***, rovibrational gateway levels; ***B***, congested levels representing a quasi-continuous bath. Solid arrows within each submanifold denote even-$|\Delta J|$ RET, and dashed arrows denote $V-V$ energy transfer. See section IV for further details.

Accompanying these regular even-$|\Delta J|$ collision-induced IR−UV DR features is a prominent series of odd-$|\Delta J|$ IR−UV DR features that is not expected in RET within a centrosymmetric molecule such as C_2H_2.[37−39] Much of this unusual odd-$|\Delta J|$ structure is centered around the $(\nu_1 + 3\nu_3)$ band $R(11)$ and $P(13)$ rovibrational features (designated by vertical arrows in the topmost part of Figure 2, at 12 699.89 and 12 641.09 cm^{-1}, respectively). It is consistent with unusually facile odd-$|\Delta J|$ collision-induced "$J_{init} = 12$ to $J_{final} = 1$" transfer to the UV PROBE-monitored $(\nu_1 + 3\nu_3)\ \Sigma_u^+\ J_{final} = 1$ level of C_2H_2 from another rovibrational level with $J_{init} = 12$ in the $4\nu_{CH}$ manifold. This relatively efficient energy transfer channel corresponds to

$\Delta J = (J_{final} - J_{init}) = -11$, which is unusual in terms of both its magnitude and its being an odd number. Another less prominent channel of odd-$|\Delta J|$ transfer appears *via* the $R(17)$ rovibrational feature in the $(\nu_1 + 3\nu_3)$ band IR−UV DR spectrum, corresponds to $\Delta J = (J_{final} - J_{init}) = -17$.

Corresponding IR−UV DR kinetic curves[39] (recorded with $P = 0.20$ Torr and the IR PUMP tuned to successive even-J_{init} peaks in the $(\nu_1 + 3\nu_3)$ band of C_2H_2) are shown in the lower right-hand column of Figure 2. The prominence and relatively rapid rise-time of the $J_{init} = 12$ kinetic curve indicate that this level acesses some form of collision-induced ET gateway. The IR−UV DR kinetic efficiency of the "$J_{init} = 12$ to $J_{final} = 1$" odd-$|\Delta J|$ transfer channel is remarkably high, comparable to that for regular $|\Delta J| = 2$ and $|\Delta J| = 4$ RET channels[37,39−42] and consistent with IR-scanned IR−UV DR spectra.[37−39] Other odd-$|\Delta J|$ transfer features fall away monotonically from the kinetic curve for $J_{init} = 12$, as if from a secondary parent peak, including the two $J_{init} = 18$ doublet components associated with the locally perturbed $R(17)$ feature at ~12 709.3 cm^{-1} that is known from IR absorption spectra;[67,68] the relatively rapid rise of IR−UV DR kinetic curves for $J_{init} = 18$ and its "perturber" indicates an additional gateway effect. Such kinetic studies of individual collision-induced IR−UV DR features therefore reveal apparent symmetry-breaking IR−UV DR signals originating from even-J_{init} levels of the $(\nu_1 + 3\nu_3)$ Σ_u^+ submanifold (notably $J_{init} = 12$) when the $(\nu_1 + 3\nu_3)$ Σ_u^+ $J_{final} = 1$ level is probed. The body of IR−UV DR kinetic results can be simulated by a phenomenological master-equation model,[40−42,69] as reported in more detail in this paper.

There is additional evidence that more than just a single discrete set of $(\nu_1 + 3\nu_3)$ Σ_u^+ J-levels contributes to IR−UV DR spectra and kinetics of the $4\nu_{CH}$ manifold, particularly when the UV PROBE is set at 299.105 nm to excite LIF *via* the $(\nu'_3 + \nu'_5)$ upper vibronic state; a highly efficient J-resolved $V-V$ transfer gateway channel is then observable, whereas that channel is not observed at 296.032 nm *via* $(\nu'_2 + \nu'_5)$.[38,39] Likewise, IR−UV DR kinetic studies in the $4\nu_{CH}$ manifold of C_2H_2 with argon (Ar) as a foreign-gas collision partner[31,39,40] verify odd-$|\Delta J|$ energy transfer as a genuine intramolecular process (as in comparable IR−UV DR studies of the ν_{CH}[48,51] and $3\nu_{CH}$[62] regions), rather than the more trivial outcome of intermolecular exchange of rovibrational excitation between *ortho* and *para* nuclear-spin modifications of C_2H_2 in self-collisions (as observed by Raman-UV DR in the ν_{CC} manifold[70] and by intermolecular "step-down" $V-V$ transfer effects in rovibrational LIF experiments[71]).

It is remarkable that collision-induced kinetics in the $4\nu_{CH}$ rovibrational manifold of C_2H_2 is complicated by an apparently ubiquitous collision-induced quasi-continuous background (CIQCB).[38−42] This unusual phenomenon is not clearly evident in the IR-scanned and kinetic IR−UV DR results of Figure 2, but it accompanies regular even-$|\Delta J|$ rovibrational energy transfer and accounts for much of the observed collision-induced odd-$|\Delta J|$ satellite structure in LIF-detected IR−UV DR spectra. It has recently been postulated[42] that the CIQCB arises from a congested array of many approximately iso-energetic IR-dark/UV-bright rovibrational levels above 12 700 cm^{-1} in the $\tilde{X}^1\Sigma_g^+$ ground electronic state of C_2H_2; this yields an effectively quasi-continuous distribution of rovibrational levels, estimated[42,69] to have a density exceeding 10 IR-dark/UV-bright levels per cm^{-1}. This is consistent with the observed CIQCB effects, which can be satisfactorily accommodated in the phenomenological model of collision-induced kinetics in the $4\nu_{CH}$ rovibrational manifold of C_2H_2,[40−42,69] as is demonstrated in this paper.

In a previous paper (part 3 of this series),[41] we have explained the systematic procedures that are involved in generating reliable IR−UV DR kinetic results such as those depicted in the lower portion of Figure 2. Processing of such J-resolved IR−UV DR kinetic data must take account of additional processes that affect the time dependence of LIF-detected IR−UV DR signals, such as collision-induced quenching of fluorescence and mass transfer from the IR−UV optical excitation zone (a combination of beam flyout and diffusion). Great experimental diligence is also required to ensure that the overall kinetic data set is internally self-consistent with respect to instrumental factors that influence IR−UV DR signal amplitude, for all values of $(V, J, K)_{init}$ and $(V, J, K)_{final}$ considered in subsequent modeling. It is necessary to make careful preparations of this type,[39,41,45,69] to obtain a self-consistent array of kinetic data for J-resolved rovibrational energy transfer channels that are to be interpreted *via* a mechanistically structured master-equation model.

III. The Rovibrational Rate-Equation Approach

We aim to deduce state-to-state rate constants and associated mechanisms from IR−UV DR kinetic measurements (e.g., as depicted in the lower portion of Figure 2) of the $4\nu_{CH}$ rovibrational manifold of C_2H_2. To do this, we implement a kinetic master-equation model of conventional form.[72] Our kinetic modeling approach is similar to that previously implemented by our group to investigate rovibrational kinetics in the 950-cm^{-1} ν_4/ν_6 manifold of D_2CO[73−76] and in the 11 600 cm^{-1} $\nu_2 + 3\nu_3$ region of C_2H_2.[45]

A vector $\mathbf{n}(t)$ is used to represent the number-density populations of a set of rovibrational levels, whose evolution in time t is defined by a matrix Π of pseudo-first-order rate constants that are generally proportional to the sample pressure P. An additional pressure-independent (but time-dependent) matrix $\delta\Pi(t)$ incorporates the effects of radiative pumping from the ground state $(V'' = 0, J'', K'')$ to an initial level $(V, J, K)_{init}$, emulating the spectroscopic action of the IR PUMP laser pulse. A set of simultaneous linear rate equations, controlling collision-induced rovibrational energy transfer from the prepared level $(V, J, K)_{init}$ to a destination level $(V, J, K)_{final}$ (as monitored at time t by the UV PROBE laser pulse), is set up in accordance with the time-resolved excitation scheme depicted in Figure 1. The kinetics may then be represented compactly in matrix form as

$$d\mathbf{n}(t)/dt = -[\Pi + \delta\Pi(t)]\cdot\mathbf{n}(t) \qquad (3)$$

It should be noted that diagonal elements Π_{ii} of the rate-constant matrix Π, correspond to the total rate constant for depletion of level i, whereas off-diagonal elements Π_{ij} of the rate-constant matrix Π, correspond to minus the rate constant for population transfer from level j to level i. The collision-induced pseudo-first-order elements Π_{ij} are related to corresponding second-order rate constants k^{ij}, because $\Pi_{ij} = k^{ij}P$. Equation 3 may be written more explicitly as

$$dn_i(t)/dt = -\sum_j [\Pi_{ij} + \delta\Pi_{ji}(t)]n_j(t) \qquad (4)$$

where i and j range over rovibrational submanifolds of interest. Solution of eqs 3 and 4 by standard computational methods yields $n_i(t)$, the population in level i at time t. Consecutive kinetic processes arising from multiple collisional interactions are included in the model, so that nonzero elements of Π are not solely allocated to transitions originating in directly pumped or probed levels.

The kinetic matrix Π is constructed in such a way that conservation, symmetry, and detailed-balance conditions[45,73] are satisfied. Detailed balance results in a nonsymmetric Π matrix because, typically

$$\Pi_{ij}\langle n\rangle_j = \Pi_{ji}\langle n\rangle_i \quad (5)$$

where $\langle n\rangle_j$ is the thermal-equilibrium population for rovibrational level j. In this work, eq 5 is altered *artificially* to yield an effective thermal equilibrium population $\langle n\rangle_j$ of level j differing from that given by a simple overall Boltzmann distribution. As will be explained more fully in section IV below, this artifice is contrived to represent a quasi-continuous distribution of rovibrational levels that is apparently consistent with the observed CIQCB effects in the $4\nu_{CH}$ rovibrational manifold of C_2H_2.[38,40−42,69] This is achieved by modifying eq 5 to include a hypothetical effective statistical weighting factor, η_j^d, for a rovibrational level j of a rovibrational submanifold d such that

$$\Pi_{ij}\langle n\rangle_j\eta_j^d = \Pi_{ji}\langle n\rangle_i\eta_i^e \quad (6)$$

where η_j^d and η_i^e depend respectively only on the rovibrational submanifolds d and e to which levels j and i belong. Note that eqs 5 and 6 allow the model to impute rate constants for downward transitions from those for upward transitions, and *vice versa*. Within any submanifold d (or e) the *same* statistical weighting factor is taken to apply to *all* rovibrational levels i (or j) of that submanifold, so that the i (or j) suffix can be suppressed, i.e., $\eta_j^d \equiv \eta^d$ (or $\eta_i^e \equiv \eta^e$).

Our model of IR−UV DR kinetics in the $4\nu_{CH}$ manifold of C_2H_2 identifies three distinct rovibrational submanifolds, as depicted schematically in Figure 3: the directly monitored (V, J, K)-levels of the $(\nu_1 + 3\nu_3)$ Σ_u^+ submanifold (to which we ascribe the label $\boldsymbol{V}$); a less well-characterized rovibrational gateway submanifold (labeled $\boldsymbol{G}$); a quasi-continuous bath (labeled $\boldsymbol{B}$). Further details of these submanifolds and of their incorporation in the kinetic model will be presented in section IV below.

For most rovibrational submanifolds, $\eta_j^d \equiv \eta^d$ (or $\eta_i^e \equiv \eta^e$) is trivially set equal to unity and the statistical weighting factors are redundant in eq 6. However, a high statistical weighting factor ($\eta_j^{\boldsymbol{B}} \equiv \eta^{\boldsymbol{B}} \gg 1$, typically $= 100$) is introduced to model energy transfer into the bath submanifold $\boldsymbol{B}$. This is because the bath is artificially represented in our model by a set of discrete levels effectively "condensed" out of the quasi-continuum (i.e., we may consider each discrete level B, J, K representing the bath $\boldsymbol{B}$ in the model to take the place of $\eta^{\boldsymbol{B}}$ actual levels of the quasi-continuous bath).

The optical pumping matrix $\delta\Pi(t)$ in eqs 3 and 4 depends on the IR−UV DR delay t and allows phenomenologically for the combined effects of IR and UV PROBE laser pulses. This comprises a rectangular pulse of 30 ns duration (which has previously been shown[45] to be consistent with optical pulse durations of approximately 8 and 15 ns fwhm for the IR PUMP and UV PROBE laser pulses respectively and a ±10 ns resolution of the digital counter used to log the IR−UV DR kinetic data). The model can then satisfactorily reproduce the rising portions (i.e., the initial 30 ns range of IR−UV delay t) in all IR−UV DR kinetic curves, particularly those of the parent or directly pumped level. An amplitude factor, proportional to the infrared pumping rate, is also incorporated in the pumping matrix $\delta\Pi(t)$.

The model is adapted to accommodate different infrared absorption line-strength factors for rovibrational levels (V, J, K)$_{init}$ prepared by the IR PUMP. This entails calibration by recording typical $(\nu_1 + 3\nu_3)$ band photoacoustic absorption spectra of C_2H_2. It has been found advantageous to adjust the relative intensity associated with the $(\nu_1 + 3\nu_3)$ Σ_u^+ $J = 1$ and 3 rovibrational levels slightly (by less than two standard deviations from mean observed photoacoustic-spectroscopic signal amplitudes) to improve fits to IR−UV DR kinetics at low values of J. Moreover, each probed level (V, J, K)$_{final}$ is LIF-monitored *via* a different UV PROBE transition, so that Hönl−London line-strength factors are required to convert IR−UV DR signal amplitudes to level populations or *vice versa*.

The kinetic model also incorporates a phenomenological rate constant k_D that allows for collision-induced energy transfer (e.g., vibrational relaxation) beyond the field of states specified in the kinetic matrix Π. As before,[45,73] this is achieved by applying a damping correction to the nonequilibrium portion of the population and multiplying the result by an exponential decay function, $\exp(-Pk_Dt)$. In cases where the $\boldsymbol{V}$ $(\nu_1 + 3\nu_3)$ and $\boldsymbol{G}$ (gateway) submanifolds are probed, we adopt a value of $k_D = 4\ \mu s^{-1}\ Torr^{-1}$ (i.e., ∼25% of 16.4 μs^{-1} $Torr^{-1}$, the Lennard-Jones collision rate constant[62]), as in our previous IR−UV DR kinetic studies.[45] However, it is found necessary to halve k_D to a value of 2 μs^{-1} $Torr^{-1}$ when the bath submanifold $\boldsymbol{B}$ is probed; this is consistent with the notion that molecules are to some extent "trapped" once in the bath $\boldsymbol{B}$ and therefore subject to a reduced damping correction. At the same point in the computational process, a factor is included for mass transport losses due to beam flyout and/or diffusion,[77] the functional form of which has been discussed and characterized in a previous paper.[41]

The microscopic form of model that best describes IR−UV DR kinetics in the $4\nu_{CH}$ rovibrational manifold of C_2H_2 is based on an exponential gap law (EGL) description of the phenomenological state-to-state rate constants involved in the Π matrix for collision-induced energy transfer. Adaptation of our previously adopted approach[45] yields a EGL relationship of form

$$\Pi_{ij} = -(\eta_i^d\langle n\rangle_i/\eta_j^e\langle n\rangle_j)^{1/2}K_0P\exp(-\alpha|\Delta E_{ij}|/k_BT) \quad (7)$$

where $|\Delta E_{ij}|$ is the energy gap and K_0 and α are fitting parameters. The factor $(\eta_i^d\langle n\rangle_i/\eta_j^e\langle n\rangle_j)^{1/2}$ satisfies the detailed-balance condition of eq 6, with η_i^d ($\equiv\eta^d$) and $\langle n\rangle_i$ as defined in that context. Equation 7 is one of several well-established relationships[57,78−80] that can be employed (with various degrees of adequacy) to define microscopic state-to-state rate constants as a function of the energy difference between initial and final levels. A power-gap scaling relationship[57,78,81] was also tested in our modeling computations, but it yields inferior results. The choice of adjustable fitting parameters K_0 and α allows mechanistic definition of the assorted channels of energy transfer that need to be incorporated into the model. In situations where $\eta^d \neq \eta^e$ (e.g., $V-V$ transfer to or from the bath $\boldsymbol{B}$), we introduce an "effective" rate constant $(\eta^d/\eta^e)^{1/2}K_0$, which incorporates the relative statistical weighting factor.

Overall, our model employs at least ten independent values of $(\eta^d/\eta^e)^{1/2}K_0$ and two of α as adjustable fitting parameters required in our model, as will be explained in section IV. For instance, the effective parameter values of $(\eta^d/\eta^e)^{1/2}K_0$ determine the extent to which the rate constant Π_{ij} for a particular channel of energy transfer depends on a J-dependent gateway mechanism, whereas the value of α determines how markedly the value of rate constant decreases with increasing energy gap $|\Delta E_{ij}|$.

In our previous investigations,[45,75,76] we have computed a goodness-of-fit variance value for each model-generated kinetic

TABLE 3: Effective Exponential Gap Law (EGL) Fitting Parameters for C_2H_2/C_2H_2 Self-Collisions at 300 K, Describing State-to-State Rotational Energy Transfer (RET) in the $4\nu_{CH}$ Rovibrational Manifold of Present Interest and Compared with Other EGL Fits to RET in Lower-Energy Rovibrational Manifolds[a]

energy transfer process of interest	effective EGL fitting parameters[b] K_0^{RET} (μs^{-1} $Torr^{-1}$)	α^{RET}	ref
Even-$\|\Delta J\|$ RET Channels within the $4\nu_{CH}$ Rovibrational Manifold of C_2H_2 at ~12 700 cm^{-1}			
$\|\Delta J\| = 2$ ("fast") RET within the iso-energetic $\boldsymbol{V}$ ($\nu_1 + 3\nu_3$) and $\boldsymbol{G}$ (gateway) submanifolds	6.0	1.8	this work
$\|\Delta J\| \geq 4$ ("slow") RET within the iso-energetic $\boldsymbol{V}$ ($\nu_1 + 3\nu_3$) and $\boldsymbol{G}$ (gateway) submanifolds	5.0	1.8	this work
$\|\Delta J\| = 2$ ("fast") equilibration in the bath ($\boldsymbol{B}$)	60[c]	1.8	this work
$\|\Delta J\| \geq 4$ ("slow") equilibration in the bath ($\boldsymbol{B}$)	50[c]	1.8	this work
Even-$\|\Delta J\|$ RET Channels within Lower-Energy Rovibrational Manifolds of C_2H_2			
RET within the ν_{CC} manifold at ~1975 cm^{-1}	4.1 ± 1.5	1.16 ± 0.15	82
RET in the $(\nu_3/\nu_2 + \nu_4 + \nu_5)_I$ ν_{CH} Fermi dyad component at ~3295 cm^{-1}	8.1 ± 0.7	1.92 ± 0.17	48
$\|\Delta J\| = 2$ ("fast") RET in the $(\nu_3/\nu_2 + \nu_4 + \nu_5)_{II}$ ν_{CH} Fermi dyad component at ~3280 cm^{-1}	11.0 ± 1.9	1.71	50
$\|\Delta J\| \geq 4$ ("slow") RET in the $(\nu_3/\nu_2 + \nu_4 + \nu_5)_{II}$ ν_{CH} Fermi dyad component at ~3280 cm^{-1}	4.8 ± 0.8	1.71	50
RET within the $3\nu_{CH}$ manifold at ~9640 cm^{-1}	6.4 ± 0.7	1.68 ± 0.03	57
$\|\Delta J\| = 2$ ("fast") RET within the ($\nu_{CC} + 3\nu_{CH}$) manifold at ~11 600 cm^{-1}	9.0	1.6	45
$\|\Delta J\| \geq 4$ ("slow") RET within the ($\nu_{CC} + 3\nu_{CH}$) manifold at ~11 600 cm^{-1}	4.0	1.6	45

[a] Relevant spectroscopic nomenclature, rovibrational energetics, and energy transfer details are systematically reviewed in ref 35. Collision-induced RET kinetics in the ν_{CC} rovibrational manifold of C_2H_2 has been measured by Raman-UV double resonance spectroscopy; the remainder of the table refers to collision-induced RET kinetic measurements by IR−UV DR spectroscopy. [b] Effective exponential gap law (EGL) fitting parameters K_0^{RET} and α^{RET} are as defined in the context of eqs 5−7. Units for an ideal gas at 300 K: 1.0 μs^{-1} $Torr^{-1}$ = 3.1 × 10^{-11} cm^3 $molecule^{-1}$ s^{-1}. [c] These effective K_0 values for RET within the bath ($\boldsymbol{B}$) are set 10 times greater than those for the iso-energetic $\boldsymbol{V}$ ($\nu_1 + 3\nu_3$) and $\boldsymbol{G}$ (gateway) submanifolds. This large effective value of K_0 artificially generates rapid collision-induced equilibration within the discretely structured $\boldsymbol{B}$ submanifold that is devised to represent the actual dense array of levels in the quasi-continuous bath, in such a way that adequately reproduces minimal induction effects in the observed IR−UV DR kinetics. However, it should not be taken to imply abnormally large state-to-state RET rate constants within the bath $\boldsymbol{B}$.

curve, to provide a quantitative measure of the agreement between experiment and model and to facilitate iterative fits. In the present work, however, the complicated (and somewhat speculative) gateway and CIQCB effects make it impractical to incorporate a goodness-of-fit value for each model-generated kinetic curve and for compilation of final fits to the observed kinetic curves. The form of the rate-equation model that best fits the observed kinetics is therefore established on the basis of an iterative series of computations, entailing assorted adaptations and modifications that are outlined in section IV below. Payne[69] has discussed other computational subtleties of our rate-equation model, as applied to collision-induced IR−UV DR kinetics in the $4\nu_{CH}$ rovibrational manifold of C_2H_2.

IV. The Rate-Constant Matrix Π for Collision-Induced Rovibrational Energy Transfer

Figure 3 schematically shows the format of the model that best fits the observed IR−UV DR kinetics in the $4\nu_{CH}$ rovibrational manifold of C_2H_2. As discussed briefly in section III, the $4\nu_{CH}$ manifold is partitioned notionally into three distinct rovibrational submanifolds ($\nu_1 + 3\nu_3$) Σ_u^+, gateway, and bath (labeled $\boldsymbol{V}$, $\boldsymbol{G}$, and $\boldsymbol{B}$, respectively) that communicate *via* collision-induced $V-V$ energy transfer.

Within each submanifold, we anticipate regular collision-induced even-$|\Delta J|$ RET within the respective submanifolds of levels (V, J, K), (G, J, K), and (B, J, K). Spectroscopic characteristics (including well-defined rotational constants, term energies, and line strengths) are abundantly available for the first of these three submanifolds ($\boldsymbol{V}$).[17,35,36−42,46,53,55,67−69] However, the other two submanifolds ($\boldsymbol{G}$ and $\boldsymbol{B}$) are inferred only indirectly from collision-induced IR−UV DR spectra. It is considered likely that the $\boldsymbol{G}$ (gateway) submanifold has particularly close coincidences in energy with the $\boldsymbol{V}$ ($\nu_1 + 3\nu_3$) submanifold between levels (V, J, K) and (G, J, K) at values of J (e.g., $J = 12$) where observed gateway effects are most pronounced and strong perturbative mixing is inferred. Moreover, all we know about the $\boldsymbol{B}$ (bath) submanifold is that it is supposedly much more congested than the $\boldsymbol{V}$ ($\nu_1 + 3\nu_3$) and $\boldsymbol{G}$ (gateway) submanifolds, as reflected by the inequality between statistical weighting factors: $\eta^{\boldsymbol{B}} \gg \eta^{\boldsymbol{V}} = \eta^{\boldsymbol{G}} = 1$ (with $\eta^{\boldsymbol{B}}$ typically set equal to 100). In the absence of more explicit spectroscopic information about the hypothetical gateway ($\boldsymbol{G}$) and bath ($\boldsymbol{B}$) submanifolds, we assume that their individual "phantom" levels (G, J, K), and (B, J, K) are iso-energetic with those of the well-characterized $\boldsymbol{V}$ ($\nu_1 + 3\nu_3$) submanifold, i.e., (V, J, K). This simple expedient provides the energy-gap values $|\Delta E_{ij}|$ that are needed to calculate elements Π_{ij} of the rate-constant matrix Π for collision-induced energy transfer, on the basis of eq 7. Any significant deficiencies in this assumption are compensated by assigning individual values of adjustable fitting parameter K_0 for particular channels of energy transfer (e.g., for the $J = 12$ gateway). It follows that, for any $V-V$ transfer process with $\Delta J = 0$, eq 7 reduces to a particularly simple isoenergetic form because $|\Delta E_{ij}| = 0$ and $\langle n \rangle_i = \langle n \rangle_j$:

$$\Pi_{ij} = -(\eta_i^d/\eta_j^e)^{1/2} K_0 P \qquad (8)$$

where (as above) $\eta_i^d \equiv \eta^d$, $\eta_j^e \equiv \eta^e$; superscripts $d \neq e$ represent $\boldsymbol{V}$ ($\nu_1 + 3\nu_3$), $\boldsymbol{G}$ (gateway), or $\boldsymbol{B}$ (bath).

As depicted in Figure 3, the two forms of collision-induced state-to-state energy transfer that occur in our kinetic model for the $4\nu_{CH}$ rovibrational manifold are (i) even-$|\Delta J|$ rotational energy transfer (RET) entirely within a given submanifold $\boldsymbol{V}$ ($\nu_1 + 3\nu_3$), $\boldsymbol{G}$ (gateway), or $\boldsymbol{B}$ (bath) and (ii) rotationally resolved vibrational ($V-V$) energy transfer between any two submanifolds $\boldsymbol{V}$, $\boldsymbol{G}$, or $\boldsymbol{B}$. In the former (even-$|\Delta J|$ RET) case, Table 3 presents the particular phenomenological EGL fitting parameters K_0^{RET} and α^{RET} for the $4\nu_{CH}$ rovibrational manifold of present interest, together with numerical values that are ultimately (see section V below) found to give a satisfactory grand fit to IR−UV DR kinetic measurements for C_2H_2/C_2H_2 self-collisions; these values are also compared with other EGL fits to even-$|\Delta J|$ RET in lower-energy rovibrational manifolds.[45,48,50,57,70] Likewise, in the latter ($V-V$) case, Table 4 presents corresponding effective EGL fitting parameters $(\eta^d/\eta^e)^{1/2}K_0^{V-V}$ and α^{V-V} for the $4\nu_{CH}$ rovibrational manifold, together with their grand-

TABLE 4: Effective Exponential Gap Law (EGL) Fitting Parameters for C_2H_2/C_2H_2 Self-Collisions at 300 K, Describing State-to-State Vibrational ($V-V$) Energy Transfer in the $4\nu_{CH}$ Rovibrational Manifold of Present Interest and Compared with Other EGL Fits to J-Resolved $V-V$ Transfer in Lower-Energy Manifolds[a]

energy transfer process of interest	effective EGL fitting parameters[b] $(\eta^d/\eta^e)^{1/2}K_0^{V-V}$ (μs^{-1} Torr^{-1})	α^{V-V}	ref
V−V Energy Transfer Channels within the $4\nu_{CH}$ Rovibrational Manifold of C_2H_2 at ~12 700 cm^{-1}			
$J = 12$ gateway transfer: $\boldsymbol{V}(\nu_1 + 3\nu_3) \leftrightarrow \boldsymbol{G}$	2.0	0.8	this work
$J = 18$ gateway transfer: $\boldsymbol{V}(\nu_1 + 3\nu_3) \leftrightarrow \boldsymbol{G}$	*0.7/4.0*[c]	0.8	this work
$V-V$ transfer at other J: $\boldsymbol{V}(\nu_1 + 3\nu_3) \leftrightarrow \boldsymbol{G}$	0.2	0.8	This work
$J = 12$ bath transfer: $\boldsymbol{B} \leftarrow \boldsymbol{V}(\nu_1 + 3\nu_3)$ or $\boldsymbol{G}$	0.3	0.8	this work
$J = 12$ bath transfer: $\boldsymbol{B} \rightarrow \boldsymbol{V}(\nu_1 + 3\nu_3)$ or $\boldsymbol{G}$	0.003	0.8	this work
$J = 18$ bath transfer: $\boldsymbol{B} \leftarrow \boldsymbol{V}(\nu_1 + 3\nu_3)$ or $\boldsymbol{G}$	*0.35/2.0*[c]	0.8	this work
$J = 18$ bath transfer: $\boldsymbol{B} \rightarrow \boldsymbol{V}(\nu_1 + 3\nu_3)$ or $\boldsymbol{G}$	*0.0035/0.02*[c]	0.8	this work
bath transfer at other J: $\boldsymbol{B} \leftarrow \boldsymbol{V}(\nu_1 + 3\nu_3)$ or $\boldsymbol{G}$	0.1	0.8	this work
bath transfer at other J: $\boldsymbol{B} \rightarrow \boldsymbol{V}(\nu_1 + 3\nu_3)$ or $\boldsymbol{G}$	0.001	0.8	this work
V−V Energy Transfer Channels within Lower-Energy Rovibrational Manifolds of C_2H_2			
$V-V$ transfer within the Fermi-type ν_{CH} dyad: $(\nu_3/\nu_2 + \nu_4 + \nu_5)_I \rightarrow (\nu_3/\nu_2 + \nu_4 + \nu_5)_{II}$	1.3 ± 0.4	1.70 ± 0.74	48
$V-V$ transfer within the Fermi-type ν_{CH} dyad: $(\nu_3/\nu_2 + \nu_4 + \nu_5)_{II} \rightarrow (\nu_3/\nu_2 + \nu_4 + \nu_5)_I$	0.9 ± 0.1	0.91 ± 0.31	50
$V-V$ transfer in the $3\nu_{CH}$ rovibrational manifold at ~9640 cm^{-1}	0.17 ± 0.01[d]	1.05 ± 0.08	57
"fast"/"slow" $V-V$ transfer in the $(\nu_{CC} + 3\nu_{CH})$ rovibrational manifold at ~11 600 cm^{-1}	0.60/0.45[e]	1.1	45

[a] Relevant spectroscopic nomenclature, rovibrational energetics, and energy transfer details are systematically reviewed in ref 35. All collision-induced $V-V$ energy transfer kinetics listed has been measured by IR−UV DR spectroscopy. [b] Effective EGL fitting parameters $(\eta^d/\eta^e)^{1/2}K_0^{V-V}$ and α^{V-V} are as defined in the context of eqs 5−8, with $\eta^{\boldsymbol{B}} = 100 \gg \eta^{\boldsymbol{V}} = \eta^{\boldsymbol{G}} = 1$. Units: $1.0\ \mu s^{-1}$ Torr$^{-1} = 3.1 \times 10^{-11}$ cm^3 molecule^{-1} s^{-1}. [c] For gateway and bath $V-V$ transfer involving the pairs of "$J = 18$"/"$J = 18$ perturber" levels, later refinement of the kinetic model uses the italicized $(\eta^d/\eta^e)^{1/2}K_0^{V-V}$ values, as explained in the text. [d] Relevant vibrational eigenstates of the $3\nu_{CH}$ rovibrational manifold are J-dependent superpositions of $3\nu_3$, $(2\nu_1 + \nu_3)$, $(\nu_1 + \nu_2 + \nu_3 + 2\nu_4)^0$, and $(\nu_1 + \nu_2 + \nu_3 + 2\nu_4)^2$ normal-mode basis states. See refs 35 and 36 for details. [e] Two distinct K_0^{V-V} values ("fast"/"slow") are needed to model the observed J-dependent IR−UV DR $V-V$ energy transfer kinetics between prominent vibrational eigenstates of the $(\nu_{CC} + 3\nu_{CH})$ rovibrational manifold, namely, $(\nu_2 + 3\nu_3)_I$, $(\nu_2 + 3\nu_3)_{II}$, and $(4\nu_2 + 3\nu_4 + 3\nu_5)^0$ [subsequently relabeled as $(\nu_2 + 3\nu_3)^0$, $(4\nu_2 + 3\nu_4 + 3\nu_5)^2$, and $(4\nu_2 + 3\nu_4 + 3\nu_5)^0$ in ref 46]. See refs 35 and 44−46 for details.

fit values (see section V below) and a comparison with other EGL fits to $V-V$ energy transfer in lower-energy rovibrational manifolds.[45,48,50,57] It should be noted that it suffices to employ a single uniform value for each of the two dimensionless EGL scaling factors: $\alpha^{RET} = 1.8$ and $\alpha^{V-V} = 0.8$. The various effective phenomenological rate-constant amplitudes K_0^{RET} and $(\eta^d/\eta^e)^{1/2}K_0^{V-V}$ (e.g., in units of μs^{-1} Torr^{-1}) can be divided simply by the Lennard-Jones rate constant k_{LJ} ($16.4\ \mu s^{-1}$ Torr^{-1}, for C_2H_2/C_2H_2 self-collisions at 300 K[62]), to convert them to corresponding dimensionless effective state-to-state collisional efficiencies P^{RET} and P^{V-V} (in the iso-energetic limit, independent of EGL scaling).

From Table 3, values of the resulting state-to-state iso-energetic collisional efficiencies $\mathscr{P}^{RET}$ for RET within the $\boldsymbol{V}$ $(\nu_1 + 3\nu_3)$ and $\boldsymbol{G}$ (gateway) submanifolds are ~0.35, whereas $\mathscr{P}^{RET}$ for iso-energetic RET within the bath $\boldsymbol{B}$ is supposed to be ~3.5 (i.e., 10 times greater); this is contrived to simulate rapid collision-induced rotational equilibration within the quasi-continuous bath, consistent with small induction effects in the observed IR−UV DR kinetics.[41,69] However, this does not necessarily imply abnormally efficient collision-induced RET between actual rotational levels of the bath submanifold.

The parameters in Table 4 yield assorted values of state-to-state iso-energetic collisional efficiencies $\mathscr{P}^{V-V}$ for J-resolved $V-V$ energy transfer in the $4\nu_{CH}$ rovibrational manifold of C_2H_2; these range from $<10^{-4}$ to ~0.25, defining the intrinsic mechanistic structure of the rate-constant matrix Π in our model.[69]

It is particularly significant that, as recognized in our recent discussions of collision-induced energy transfer in the $4\nu_{CH}$ rovibrational manifold of C_2H_2,[35,42] the apparent odd-$|\Delta J|$ processes observed in IR−UV DR spectra and kinetics can be ascribed entirely to $V-V$ transfer between the quasi-continuous bath $\boldsymbol{B}$ and the discrete J-levels of the $\boldsymbol{V}$ $(\nu_1 + 3\nu_3)$ submanifold (with the gateway submanifold $\boldsymbol{G}$ also possibly implicated). Our phenomenological kinetic model therefore does not need at any stage to invoke odd-$|\Delta J|$ RET; this would have implied breaking of *a*/*s* nuclear-spin symmetry and interconversion of *ortho* ($I = 1$, *a*) and *para* ($I = 0$, *s*) nuclear-spin modifications of C_2H_2, which is unlikely to occur on the time scale of our IR−UV DR experiments. In fact, the kinetic master-equation model treats supposed "even-J" and "odd-J" rotational levels in separate, independent blocks of the rate-constant matrix Π and (as demonstrated in section V) satisfactorily fits the observed apparent odd-$|\Delta J|$ processes in IR−UV DR kinetics. Detailed mechanistic implications are further discussed in section VI.

V. Phenomenological Rate-Equation Fits to IR−UV DR Kinetics

A major outcome of this paper is that our phenomenological master-equation model can satisfactorily simulate an extensive body of available IR−UV DR kinetic results for collision-induced energy transfer in the $4\nu_{CH}$ rovibrational manifold of C_2H_2, as previously reported in less detail.[40,41] These data are assembled from four measured sets of averaged IR−UV DR kinetic curves, each with the IR PUMP tuned successively to prepare the $(\nu_1 + 3\nu_3)$ $J_{init} = 1-19$ levels and with the UV PROBE wavelength (λ_{UV}) set selectively at ~299 nm to monitor features that are unambiguously characteristic *either* of discrete J_{final} levels in the $\boldsymbol{V}$ $(\nu_1 + 3\nu_3)$ submanifold *or* of the quasi-continuous bath $\boldsymbol{B}$, as follows: ***Set A***, as in Figure 2 above, with $\lambda_{UV} = 299.105$ nm, probing the $(\nu_1 + 3\nu_3)$ $J_{final} = 1$ level;[37,39] ***Set B***, with $\lambda_{UV} = 299.452$ nm, probing the $(\nu_1 + 3\nu_3)$ $J_{final} = 12$ level;[38,41] ***Set C***, with $\lambda_{UV} = 298.973$ nm, probing the $(\nu_1 + 3\nu_3)$ $J_{final} = 17$ doublet;[40] and ***Set D***, with $\lambda_{UV} = 298.767$ nm, off-resonance from any discrete $(\nu_1 + 3\nu_3)$ J_{final} levels and thereby sampling the kinetics of the underlying CIQCB bath alone.[38,42]

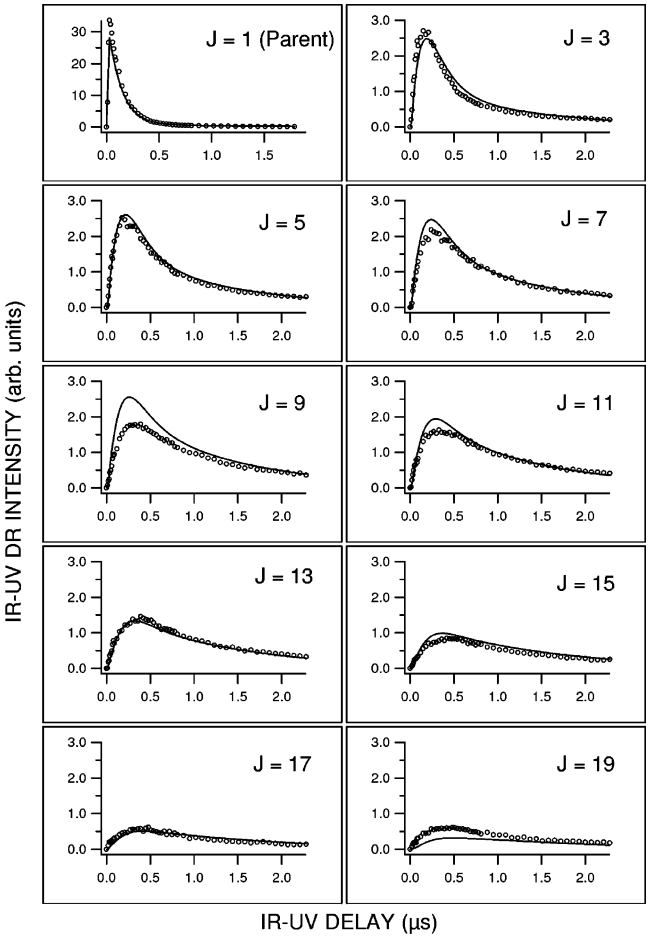

Figure 4. IR−UV DR kinetic curves for ***Set A***, corresponding to collision-induced even-$|\Delta J|$ transfer between $J_{final} = 1$ and $J_{init} = 1-19$ in the $\boldsymbol{V}$ ($\nu_1 + 3\nu_3$) submanifold of C_2H_2 ($P = 0.20$ Torr). Open circles represent observed reduced kinetic curves (e.g., derived from the left-hand column of Figure 2). Basic model-generated solid lines are compiled by adding even-$|\Delta J|$ background-subtracted kinetic curves for ***Set A*** to corresponding reduced kinetic curves of the CIQCB bath from ***Set D***.

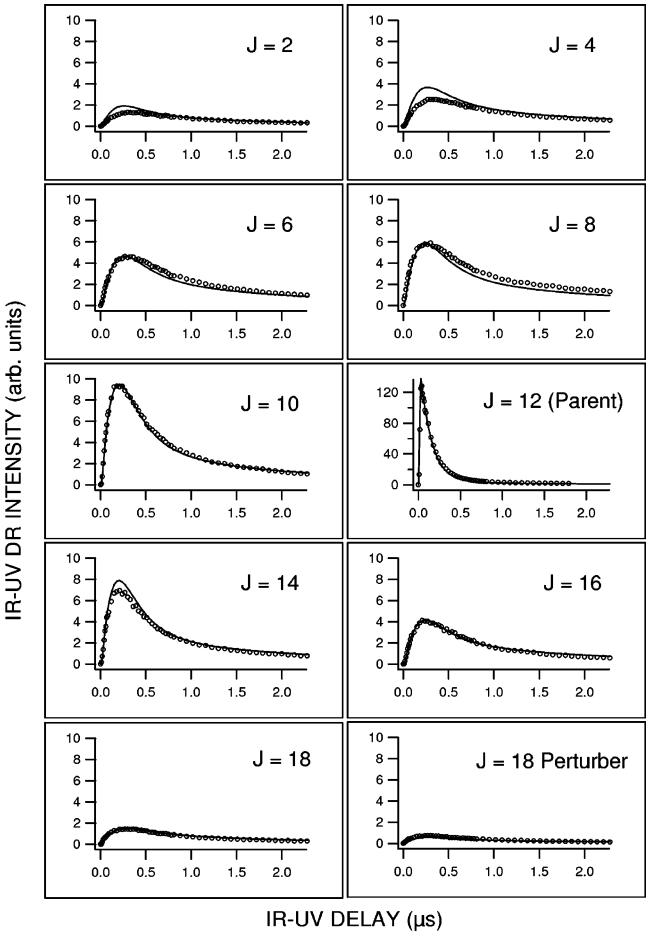

Figure 5. IR−UV DR kinetic curves for ***Set B***, corresponding to collision-induced even-$|\Delta J|$ transfer between $J_{final} = 12$ and $J_{init} = 2-18$ in the $\boldsymbol{V}$ ($\nu_1 + 3\nu_3$) submanifold of C_2H_2 ($P = 0.20$ Torr). Open circles represent observed reduced kinetic curves (e.g., derived from the right-hand column of Figure 2 in reference 41). Basic model-generated solid lines are compiled by adding odd-$|\Delta J|$ background-subtracted kinetic curves for ***Set B*** to corresponding reduced kinetic curves of the CIQCB bath from ***Set D***.

As explained elsewhere,[41] all kinetic data are carefully standardized, signal-averaged, and reduced prior to modeling. This procedure is applied to kinetics of $\boldsymbol{V}$ ($\nu_1 + 3\nu_3$) J_{init}-levels, including parent decay (e.g., $J_{init} = J_{final} = 1$,[37,39] 12,[38,40,41] or 17[40]), even-$|\Delta J|$ and odd-$|\Delta J|$ transfer (e.g., $J_{init} \rightarrow J_{final} = 1$[37,39] or 12,[38,41] or 17[40]), and transfer between the quasi-continuous CIQCB bath and discrete levels ($J_{init} = 1-19$) of the ($\nu_1 + 3\nu_3$) submanifold.[42] It yields several forms of J_{init}-resolved kinetic curve, as follows:

- raw kinetic curves, recorded directly with optimal signal-to-noise ratio in a self-consistent fashion;[41]
- averaged kinetic curves, as in Figure 2 and ***Sets A−D*** above, derived from raw kinetic curves;[37,39−42]
- reduced kinetic curves, generated by using a sampling grid to contract averaged kinetic curves (encompassing all observed data points) to a tractable set of ∼50 data points for further analysis;[41]
- background subtracted kinetic curves, in which reduced kinetic curves for ***Set D*** (originating from the CIQCB bath) are subtracted from reduced kinetic curves for ***Sets A−C*** (which is understood[35,41,42] to be a superposition of concurrently monitored IR−UV DR signals for the CIQCB bath as well as discrete, J_{final}-probed energy transfer), in readiness for modeling of the J_{init}-resolved kinetics.[42]

Figures 4−6 demonstrate the overall quality of fit of our phenomenological kinetic model (solid lines, compiled by adding background-subtracted kinetic curves from ***Sets A−C*** to reduced kinetic curves of the CIQCB bath from ***Set D***) to observed results (open circles), for even- and odd-$|\Delta J|$ transfer with $J_{final} =$ 1 and 12; a corresponding set of kinetic curves for even-$|\Delta J|$ transfer with $J_{final} = 17$ has been depicted in a previous paper (part 2 of this series).[40] Likewise, Figure 7 shows the model-generated fit to reduced kinetic curves for transfer from even-J_{init} levels of the $\boldsymbol{V}$ ($\nu_1 + 3\nu_3$) submanifold to the CIQCB bath ***B***.

An essential feature of our phenomenological treatment of IR−UV DR spectroscopy and kinetics, for collision-induced rovibrational energy transfer within the $4\nu_{CH}$ manifold of C_2H_2, is the notion that the ubiquitous CIQCB bath ***B*** is probed at all UV PROBE wavelengths. These include those of apparently discrete rovibronic transitions chosen to monitor population in the ($\nu_1 + 3\nu_3$) rovibrational levels with $J_{final} = 1$, 12, and 17 (corresponding to ***Sets A***, ***B***, and ***C***, respectively). In effect, our IR−UV DR kinetic curves (e.g., those in Figures 4 and 5 here and in Figure 10 of ref 40) simultaneously entail transfer *not only* to a primary rovibrational level (V, J, K) of the ($\nu_1 + 3\nu_3$) $\boldsymbol{V}$ submanifold *but also* to representative iso-energetic levels (B, J, K) that are contrived in our master-equation model to represent the CIQCB bath ***B***.

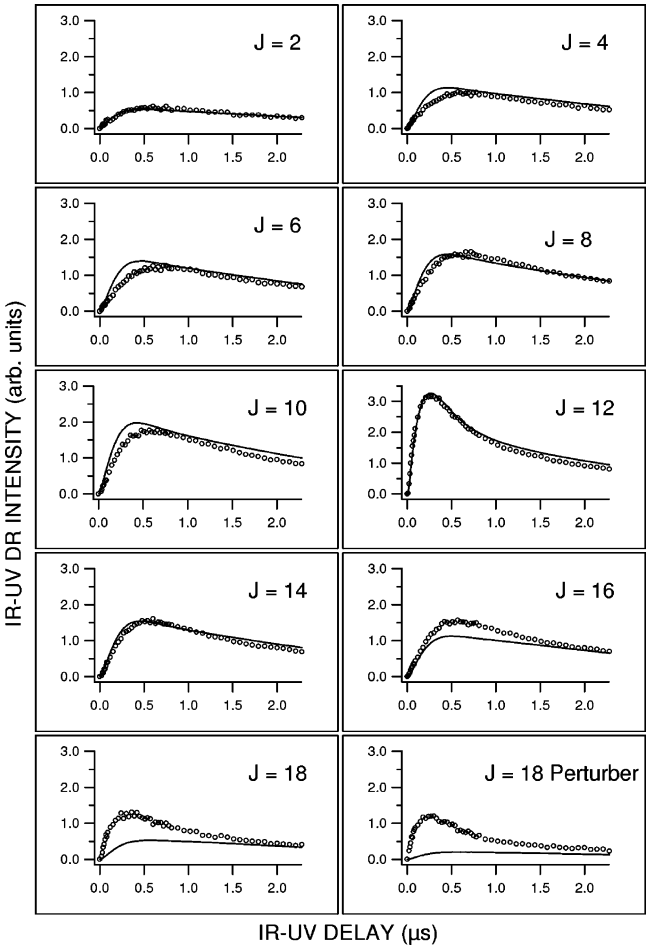

Figure 6. IR−UV DR kinetic curves for ***Set A***, corresponding to collision-induced odd-$|\Delta J|$ transfer between $J_{final} = 1$ and $J_{init} = 2-18$ in the ***V*** ($\nu_1 + 3\nu_3$) submanifold of C_2H_2 ($P = 0.20$ Torr). Open circles represent observed reduced kinetic curves (e.g., derived from the right-hand column of Figure 2). Basic model-generated solid lines are compiled by adding odd-$|\Delta J|$ background-subtracted $J = 12$ gateway kinetic curves for ***Set A*** to corresponding reduced kinetic curves of the CIQCB bath from ***Set D***.

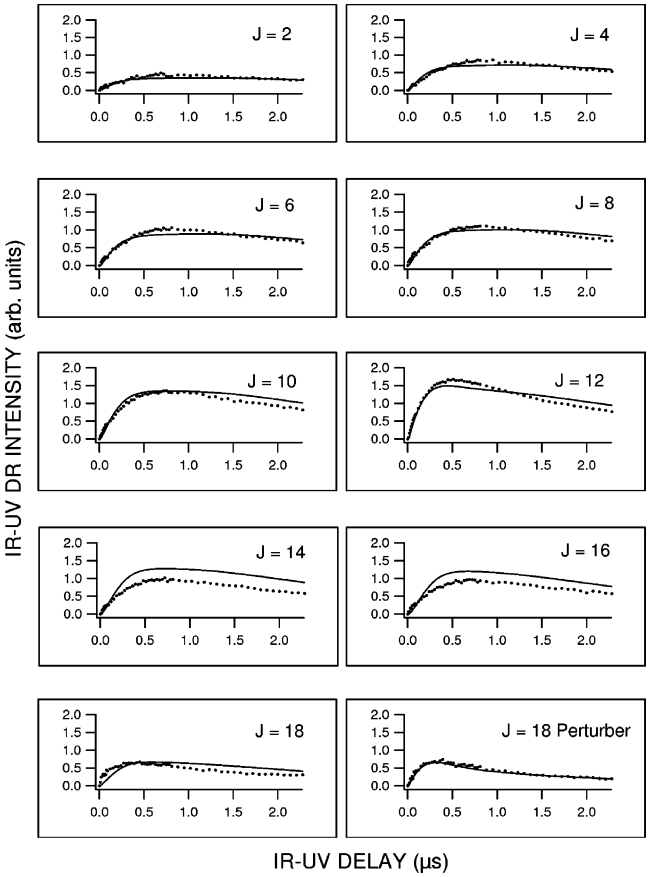

Figure 7. IR−UV DR kinetic curves for ***Set D***, corresponding to collision-induced even-J_{init} features with $J_{init} = 2-18$, prepared by the IR PUMP and LIF-monitored *via* the CIQCB bath ***B***, with the UV PROBE off-resonance from any discrete J_{final} level in the ***V*** ($\nu_1 + 3\nu_3$) submanifold of C_2H_2 ($P = 0.20$ Torr). Dots represent observed reduced kinetic curves (e.g., derived from the right-hand column of Figure 7 in ref 42). Model-generated solid lines are derived for ***Set D*** with even J_{init}, by assuming arbitrarily that the bath ***B*** is probed at its $J = 10$ level and enhanced by including $J = 18$ gateway transfer (using italicized EGL parameters from Table 4) as well as "basic" $J = 12$ gateway transfer.

The observed IR−UV DR kinetic curves compiled for ***Sets A−C*** are therefore taken to arise from a superposition of concurrent processes, allowing a portion of the signal that originates from the bath to be subtracted as a background from such kinetic curves so that the concurrent kinetic processes can be separated to enable kinetic modeling. The kinetic curves of ***Set D*** (with the off-resonance UV PROBE wavelength set at 298.767 nm, as in Figure 7 of this paper and in Figure 7 of ref 42) are used for this purpose, because the CIQCB kinetics has been found[69] to be insensitive to UV PROBE wavelength. This uniformity of the bath kinetics is borne out by the general similarity of odd-$|\Delta J|$ collision-induced features in all of our IR-scanned IR−UV DR spectra recorded at different UV PROBE wavelengths.[37−42]

It is found[41] that CIQCB bath contributions are predominant in the tail ($t > 1$ μs) of virtually all IR−UV DR kinetic curves (both even-$|\Delta J|$ and odd-$|\Delta J|$) and that background-subtracted kinetic curves for ***Sets A***, ***B***, and ***C*** approach zero asymptotically at large t without adjustment of any scaling parameter. This confirms background subtraction as an appropriate way to treat much of the odd-$|\Delta J|$ transfer kinetics.

As previously mentioned in sections III and IV and explained elsewhere,[41,69] mass transfer losses due to beam flyout and/or diffusion[77] can be factored out from the collision-induced energy transfer processes that are of primary interest here. This procedure reveals unusually rapid collision-induced transfer to the CIQCB bath ***B*** from the ($\nu_1 + 3\nu_3$) $J_{init} = 12$ level (as in Figure 7), whereas such transfer from other ($\nu_1 + 3\nu_3$) J_{init} levels is less efficient and exhibits a short (<0.5 μs) induction period that is indicative of consecutive kinetics (e.g., *via* the gateway submanifold ***G***).

The key mechanistic role of the $J = 12$ rovibrational level in the ($\nu_1 + 3\nu_3$) ***V*** submanifold was first perceived, as in the topmost portion of Figure 2, in the context of IR-scanned IR−UV DR spectra, recorded with fixed IR−UV delay t.[37−42] The pivotal role of this $J = 12$ level is also evident in the growth and decay of even-J_{init} kinetic features, associated with the ($\nu_1 + 3\nu_3$) submanifold, of ***Set A*** (probing $J_{final} = 1$; Figures 2 and 6), ***Set C*** (probing $J_{final} = 17$; Figure 8 of ref 40), and ***Set D*** (probing the CIQCB bath ***B***; Figure 7 of this paper and Figure 7 of ref 42). This applies for collision-induced transfer from the ($\nu_1 + 3\nu_3$) $J_{init} = 12$ level *not only* to the CIQCB bath ***B*** (as in Figure 7) *but also* to the ($\nu_1 + 3\nu_3$) $J_{final} = 1$ level *via* the postulated gateway submanifold ***G*** (as in Figure 6). Within all of these sets of even-J_{init} kinetic curves, the $J_{init} = 12$ feature exhibits the steepest rise and peaks several hundred nanoseconds earlier than any other curves within that set. Dominant collision-induced transfer channels *via* the $J = 12$ level, involving both

the bath (***B***) and gateway (***G***) submanifolds, have therefore been incorporated in the phenomenological master-equation model (see Table 4). As explained below, the fit to higher-*J* kinetic curves is improved by introducing a second set of gateway- and bath transfer channels involving the $J = 18$ doublet (with italicized kinetic parameters as in Table 4). Kinetic fits including only the dominant $J = 12$ gateway channel (as in Figures 4−6) are referred to as "basic", whereas those including also the $J = 18$ doublet gateway channel (as in Figure 7) are said to be "enhanced".

As depicted schematically in Figure 3, the gateway (***G***) and bath (***B***) submanifolds are contrived in our kinetic model to be iso-energetic with the well-characterized ($\nu_1 + 3\nu_3$) submanifold ***V***. Because the representative rovibrational levels (*G*, *J*, *K*) and (*B*, *J*, *K*) of the gateway (***G***) and bath (***B***) submanifolds are inferred indirectly from collision-induced IR−UV DR kinetics, there is no way to establish value(s) of J_{final} at which they may be monitored by a given UV PROBE wavelength. Submanifolds ***G*** and ***B*** are therefore assumed arbitrarily in our kinetic model to be sampled by the UV PROBE at $J_{final} = 9$ and 10, i.e., at the respective peaks of the odd- and even-*J* Boltzmann distributions for thermal equilibrium at $T = 300$ K. In the case of the bath ***B***, the predicted kinetics is found[69] to be insensitive to sampled value(s) of J_{final}, in view of rapid rotational equilibration that prevails within that submanifold (see Table 3). A similar insensitivity to sampled value(s) of J_{final} has also been verified[69] in the case of the gateway submanifold ***G***.

The amplitudes of model-generated fits to experimental IR−UV DR kinetics probing the bath (***B***) and gateway (***G***) submanifolds were adjusted to match our experimental kinetic curves because the cross sections for excitation of LIF of these submanifolds cannot be calibrated. Modeling relevant IR−UV DR kinetic data therefore aimed to reproduce the shape (e.g., rise and decay rates and peak position) of kinetic curves rather than their (uncalibrated) absolute amplitudes. A single "effective" LIF cross section has been assumed in modeling both odd-*J* and even-*J* kinetics for ***Set D*** (probing the CIQCB bath ***B***). The absolute amplitudes of model-generated kinetic curves for the bath kinetics of ***Set D*** required adjustment by an adjustable factor that varied greatly according to the value of η (the statistical weighting applied to the bath ***B***). With $\eta = 100$, it was found that the overall LIF cross sections of the bath ***B*** and gateway submanifold ***G*** were (plausibly) of the same order of magnitude as those of rovibrational levels in the well-characterized ($\nu_1 + 3\nu_3$) submanifold ***V***. Note that off-resonance IR−UV DR kinetics as in Figure 7 (and, before that, in Figures 7 and 9 of ref 42) confirm that CIQCB signals are truly collision-induced: they are zero when $t = 0$ and grow in as t and z increase.

Our phenomenological kinetic model confirms many of the mechanistic inferences made from experimental observation, such as the apparent gateway role of the $J = 12$ level and the $J = 18$ doublet of the ($\nu_1 + 3\nu_3$) rovibrational submanifold. Construction of the rate-constant matrix Π for collision-induced energy transfer is an intricate process; see sections III and IV, notably Figure 3, eqs 3−7, and Tables 3 and 4. Nevertheless, model-predicted rate constants for overall state-to-field collision-induced depletion compare favorably with experiment. For instance, the model-predicted rate constants for decay of the ($\nu_1 + 3\nu_3$) parent levels with $J = 1$ and $J = 12$ are 32 and 29 μs^{-1} $Torr^{-1}$, compared with experimentally determined values[41] of 39 ± 1 and 32 ± 1 μs^{-1} $Torr^{-1}$, respectively. This level of agreement encourages confidence that most significant channels of collision-induced state-to-state transfer are realistically identified in the cases of ***Sets A*** and ***B***.

From Figures 4−6 for ***Sets A*** and ***B*** (probing $J_{final} = 1$ and 12, respectively), from Figure 7 for ***Set D*** (probing the CIQCB bath ***B***), and from Figure 10 of ref 40 for ***Set C*** (probing $J_{final} = 17$), it is evident that our phenomenological master-equation model can yield a remarkably good global fit to the observed IR−UV DR results with a minimal number of physically realistic fitting parameters for state-to-state transfer kinetics (see Tables 3 and 4), despite their inevitable complexity.

As previously reported,[40] the compiled basic model fits to kinetic curves for ***Sets A*** and ***B*** are generally better than those for ***Set C***, where observed kinetic curves for most values J_{init} decay more rapidly than the model prediction, although the population amplitudes are generally well reproduced. It therefore appears[40] that, as for $J = 12$ and for the $J = 18$ doublet, the unresolved $J = 17$ doublet should be treated as an additional gateway for transfer to the CIQCB bath ***B*** and/or the gateway submanifold ***G***.

The CIQCB bath ***B*** provides a background to all of our IR−UV DR kinetic curves for collision-induced rovibrational energy transfer within the $4\nu_{CH}$ manifold of C_2H_2, as in Figures 4−7 (for ***Sets A***, ***B***, and ***D***) and Figure 10 of ref 40 (***Set C***). There is remarkably good agreement in Figure 7 (for ***Set D***, probing the CIQCB bath ***B***) between enhanced model-predicted kinetic curves and reduced kinetic curves from experiment. This belies the intrinsic difficulty of accommodating IR−UV DR signal contributions that arise from various consecutive processes monitored by the UV PROBE and sampled as an average over many *J*-levels of the bath submanifold ***B***, with UV-bright population cascading through the rovibrational levels of the bath. The satisfactory match in Figure 7 between model-generated kinetic curves and corresponding experimental kinetic curves at long IR−UV delays ($t > 2$ μs) reflects our hypothesis that rotational population is rapidly equilibrated once it reaches the bath.

It is useful at this stage to summarize salient features of the phenomenological master-equation model that are needed to arrive at the quality of fit that is achieved for basic compiled collision-induced IR−UV DR kinetic curves with $J_{final} = 1$ (Figures 4 and 6; ***Set A***), $J_{final} = 12$ (Figure 5; ***Set B***), and $J_{final} = 17$ (Figure 10 of reference 40; ***Set C***), as well as enhanced kinetic curves for the CIQCB bath ***B*** that is monitored by off-resonance probing (Figure 7; ***Set D***). These features may be itemized as follows:

- As explained above, the contrasting kinetics of *J*-resolved energy transfer with even $|\Delta J|$ (which conserves *a*/*s* nuclear-spin exchange symmetry of C_2H_2) and odd $|\Delta J|$ (which is apparently forbidden in the case of simple RET) are considered[41,42] to be separable and independent in the cases of ***Sets A***−***C***, with the latter (odd-$|\Delta J|$) form of transfer attributable to mechanisms involving the CIQCB bath ***B***.
- *J*-resolved modeling of the even-$|\Delta J|$ rovibrational transfer is achieved by fits to the background-subtracted kinetic curves for ***Sets A***, ***B***, and ***C*** ($J_{final} = 1$, 12, and 17, respectively). As explained above, these are free of ubiquitous underlying contributions from the CIQCB bath ***B***, which are themselves obtained from ***Set D*** and insensitive to choice of the UV PROBE wavelength that is off-resonance from any discrete J_{final} level in the ($\nu_1 + 3\nu_3$) submanifold.[69]
- The ($\nu_1 + 3\nu_3$) $J = 12$ level plays a distinctive, enabling role in collision-induced transfer to *either* the gateway submanifold ***G*** (as in Figure 6) *or* the bath ***B*** (as in Figure 7), but the growth and decay of its IR−UV DR kinetics is different in

each case. One one hand, the rise time of the odd-$|\Delta J|$, $J_{init} = 12$ feature of ***Set A*** (as in Figures 2 and 6) is unusually high, compared to that for regular $|\Delta J| = 6$ RET (as in Figures 2 and 4); this is attributed largely to highly efficient $V-V$ transfer *via* the gateway submanifold ***G***, with kinetic parameters $(\eta^d/\eta^e)^{1/2}K_0^{V-V}$ and α^{V-V} as in Table 4. On the other hand, the $J_{init} = 12$ feature of ***Set D*** (as in Figure 7 of this paper and in Figure 7 of ref 42) rises less rapidly than the corresponding feature in ***Set A***; this indicates that direct $V-V$ transfer to the bath ***B*** is only moderately efficient, consistent with kinetic parameters $(\eta^d/\eta^e)^{1/2}K_0^{V-V}$ and α^{V-V} as in Table 4.

•As discussed above, the $(\nu_1 + 3\nu_3)$ $J_{init} = 12$ rovibrational level of ***Set A*** (see Table 4) is not an exclusive gateway for highly efficient collision-induced transfer, in that there are other less prominent gateways, such as that involving the $(\nu_1 + 3\nu_3)$ $J = 18$ rovibrational level and its accompanying perturber level (with italicized kinetic parameters as in Table 4). The enhanced master-equation model (including the $J = 18$ doublet channel) provides a significantly improved fit to the observed kinetics for ***Set A*** (as in the high-J_{init} portion of Figure 7) and resolves apparent discrepancies. For instance, it yields a superior fit to observed IR−UV DR transfer kinetics for ***Set D*** in the case of the $J_{init} = 18$ level and its perturber (as in Figure 6), compared to the poor fit generated by the basic model for odd-$|\Delta J|$ transfer from the $J_{init} = 18$ doublet of ***Set A*** in Figure 6. However, agreement between observed and modeled kinetics remains deficient in the high-J limit, with regard to overall complexity of the problem, the lack of sufficiently detailed spectroscopic information, and the need for a more adequate treatment of collision-induced effects involving the perturbed $J_{init} = 18$ doublet levels.

VI. Concluding Remarks: Mechanistic Implications

To conclude, we address two mechanistic questions concerning collision-induced kinetics of energy transfer in the $4\nu_{CH}$ rovibrational manifold of C_2H_2, investigated by IR−UV DR spectroscopy, namely:

A. What characteristic spectroscopic assignments apply to the bath (***B***) and gateway submanifold (***G***)?

B. What are the implications of these results for C_2H_2 in the wider context of molecular physics?

In considering question A, it should be recognized that much is already known[35,36,67−69] about the spectroscopy and energetics of the IR-bright $(\nu_1 + 3\nu_3)$ rovibrational levels in the $4\nu_{CH}$ manifold of C_2H_2 at ~12 700 cm^{-1}. However, the accompanying IR-dark gateway (***G***) and bath (***B***) submanifolds are inferred only on phenomenological grounds *via* their apparent manifestation in the IR−UV DR kinetic mechanisms that are explored in this paper; their specific nature is therefore much more speculative.

The origins of the collision-induced quasi-continuous background (CIQCB), that is found[38,42] to underlie the discrete J-resolved structure of collision-induced IR−UV DR spectra in the $4\nu_{CH}$ region, remain a mystery. Nevertheless, the CIQCB is interpreted[35,38,42] on the basis of our systematic IR−UV DR spectroscopic experiments and proposed[41,42] to be equivalent to the bath submanifold ***B*** that is an essential element of the phenomenological kinetic model presented in this paper. Note that comparable CIQCB effects are observed in *both* C_2H_2/C_2H_2 self-collisions *and* C_2H_2/Ar collisions, which effectively rules out the possibility of an intermolecular transfer mechanism.[42] The CIQCB bath is postulated mechanistically[35,42] to arise from a congested array of IR-dark/UV-bright rovibrational levels in the $\tilde{X}^1\Sigma_g^+$ electronic ground state of C_2H_2; the estimated[69] density of available IR-dark/UV-bright rovibrational levels exceeds 10 levels per cm^{-1}, on the basis of all vibrational levels (both *gerade* and *ungerade*) with polyad quantum number $n_{res} = 20$ and vibrational angular momentum quantum number $l = 0-3$, and is effectively enhanced by rapid collision-induced RET. The CIQCB bath is taken to be populated by collision-induced energy transfer after IR PUMP excitation, followed by LIF-detected UV PROBE $\tilde{A}-\tilde{X}$ rovibronic absorption. Many of the approximately isoenergetic rovibrational levels at ~12 700 cm^{-1} that may contribute to the CIQCB have $l > 0$, with Π, Δ, Φ, ... character that causes J-levels to occur in l-type doublets with e- and f-symmetry components;[83] this allows collision-induced rovibrational transfer (e ↔ f) with odd $|\Delta J|$ as well as even $|\Delta J|$ without needing to invoke *a*/*s* nuclear-spin symmetry breaking and interconversion of *ortho* and *para* nuclear-spin modifications of C_2H_2.[37,39]

Several J-specific gateways for collision-induced energy transfer have been identified in the course of IR−UV DR studies of C_2H_2 in its 12 700 cm^{-1} $4\nu_{CH}$ rovibrational manifold. The mechanisms of these are understood in terms of a gateway submanifold ***G*** containing discrete IR-dark/UV-bright rovibrational levels that are nearly isoenergetic with discrete IR-bright rovibrational levels in the $(\nu_1 + 3\nu_3)$ submanifold ***V*** and the CIQCB bath submanifold ***B***. The most prominent of these gateways involves the $(\nu_1 + 3\nu_3)$ $J = 12$ rovibrational level and is invoked (in addition to relaxation to the CIQCB bath ***B***) to model the spectroscopy and kinetics of unusually complicated odd-$|\Delta J|$ transfer from $J_{init} = 12$ to $J_{final} = 1$,[38−42,69] as illustrated in Figure 6. This gateway channel comprises $V-V$ transfer to an IR-dark vibrational level that is tentatively assigned by a rovibrational polyad model[45,46] as $(3\nu_2 + 10\nu_4 + \nu_5)/(\nu_1 + 2\nu_3 + 4\nu_4 + \nu_5)$, with $\Pi_u^{(e)}$ $(l = 1)$ symmetry, $n_{res} = 20$, and mixed vibrational basis state parentage.[38,42,45,46,69] Less prominent secondary gateway channels, involving the main and perturber levels of the $(\nu_1 + 3\nu_3)$ rovibrational doublets with $J = 18$ and 17, are also recognized;[40−42,68,69] these have been discussed (but not identified, even tentatively) in section V above.

It is therefore important to acknowledge the phenomenological nature of our J-resolved master-equation model of collision-induced kinetics in the $4\nu_{CH}$ rovibrational manifold of C_2H_2. The model is devised hypothetically to optimize the overall agreement with observed IR−UV DR kinetic curves. It is based on spectroscopic and dynamical information that is not as detailed as might be desired (or expected, in the case of a simpler molecule or in less highly excited rovibrational manifolds of C_2H_2). Our kinetic model might, therefore, be less than unique in describing some of the intrinsic physical processes that remain open to conjecture.

We now consider the latter of the above two major mechanistic issues, framed as question **B** concerning the general relevance and implications of our IR−UV DR experimental results for C_2H_2. There is an extensive body of IR-absorption data for gas-phase C_2H_2,[35,36,64,65,67,68,84] but this by itself cannot provide information on IR-dark rovibrational levels that are of central interest to us.

Various laser-spectroscopic techniques are available to monitor J-resolved energetics and collision-induced transfer in congested high-energy rovibrational manifolds of C_2H_2. The action of each of these techniques can be distinguished from that of our time-resolved, LIF-detected IR−UV DR spectroscopic approach. This is because IR−UV DR spectroscopy alone employs Franck−Condon factors associated with UV PROBE excitation to project out IR-dark/UV-bright rovibrational levels $(V, J, K)_{final}$ that are populated by collision-induced transfer from

IR-bright rovibrational levels $(V, J, K)_{init}$ selectively prepared by the IR PUMP. Several other versatile Franck−Condon-assisted detection techniques, including stimulated emission pumping[85] and dispersed rovibronic LIF,[86,87] are also useful in elucidating the high-energy rovibrational manifolds of C_2H_2. However, none of these approaches have the distinctive capability of IR−UV DR spectroscopy to reveal the combined IR and UV darkness/brightness of rovibrational levels involved in collision-induced energy transfer.[63]

Moreover, dispersed rovibrational LIF measurements of C_2H_2 excited in the 12 700 cm^{-1} $4\nu_{CH}$ and 11 600 cm^{-1} $(\nu_{CC} + 3\nu_{CH})$ regions have been made by Halonen and co-workers,[88,89] where observed odd-$|\Delta J|$ collision-induced satellite features are attributed to *inter*molecular vibrational step-down processes that scramble the *ortho* and *para* nuclear-spin modifications of C_2H_2, but without needing to break the strongly conserved *a*/*s* nuclear-spin symmetry.[89] There is no sign in these dispersed rovibrational LIF measurements[89] of the CIQCB and/or *intra*molecular odd-$|\Delta J|$ transfer phenomena that are observed in our IR−UV DR experiments employing rovibronic LIF detection.[37−46] However, this may be attributable to the low sensitivity of rovibrational LIF relative to that of rovibronic LIF.

Several additional indirect spectroscopic techniques, entailing assorted forms of molecular action that are generally more complicated than simple absorption or emission of radiation, can be used to address processes in the $4\nu_{CH}$ rovibrational manifold of C_2H_2 at ~12 700 cm^{-1}. These include optothermally detected molecular-beam laser-Stark spectroscopy[16,17] (which has synergy with IR−UV DR spectroscopy in the $(\nu_{CC} + 3\nu_{CH})$ and $4\nu_{CH}$ manifolds[35,37−46]) and pulsed two-step IR−UV excitation of dissociative H-atom action spectroscopy.[90] In particular, the local perturbation that causes doublet splitting of the $J = 17$ and $J = 18$ levels in the $(\nu_1 + 3\nu_3)$ submanifold has been assigned[40,68] in terms of a crossing between the Coriolis-coupled zero-order levels of the IR-bright, UV-dark $(\nu_1 + 3\nu_3)$ Σ_u^+ submanifold and of the IR-dark, UV-bright $(5\nu_2 + 4\nu_4 + \nu_5)$ $\Pi_u^{(e)}$ submanifold. Possible links, between such intramolecular perturbations and anomalous collision-induced rovibrational energy transfer within the $4\nu_{CH}$ manifold of C_2H_2, have been examined[40] by measuring time-resolved, LIF-detected IR−UV DR spectra with the IR PUMP preparing either or both of the $(\nu_1 + 3\nu_3)$ $J = 17$ and $J = 18$ doublet levels. These appear as locally perturbed doublets in IR absorption spectra[67,68] (with unusually large collision-induced lineshifts[67,91]), in IR−UV DR spectra,[37−42,69,92] and in vibrationally mediated photodissociation action spectra[89] (with large photodissociation cross sections[89]). This assortment of direct and indirect spectroscopic methods, applicable to rovibrational transfer processes in C_2H_2, has been reviewed in our recent papers.[35,39−42] It is thereby possible to view interesting rovibrational phenomena, such as local perturbations and associated dynamical processes, from several aspects and compare them with our IR−UV DR results. However, these assorted experimental methods (including collision-induced dispersed rovibrational LIF[89]) fail to reproduce distinctive phenomena (e.g., CIQCB and/or odd-$|\Delta J|$ transfer) revealed by IR−UV DR. This reflects the relatively high sensitivity and state-specificity that derives from the temporal sequence of IR PUMP, UV PROBE, and UV LIF detection adopted in our time-resolved IR−UV DR technique.

Finally, there are interesting parallels between our gas-phase IR−UV DR experiments and various applications of optothermal spectroscopy by Gough, Lehmann, Miller, Scoles, Watts, and co-workers. This includes the already-mentioned interplay between gas-phase IR−UV DR and optothermally detected molecular-beam laser-Stark spectroscopy[16,17] that initially stimulated our interest in the $(\nu_{CC} + 3\nu_{CH})$ and $4\nu_{CH}$ manifolds of C_2H_2,[35,37−46] Structural and spectroscopic properties of molecular complexes and clusters of C_2H_2, as determined by Miller and co-workers,[2,10a,11,14b,14c,21c,93−95] have recently been reviewed.[35] Also presented[35] is a corresponding review of C_2H_2 and its complexes incorporated in He nanodroplets[34,96]—a fascinating frontier of molecular spectroscopy and dynamics.[30−34]

A topical theme of optothermal spectroscopy, relevant to issues addressed in our IR−UV DR studies, is the extent to which prominent intramolecular perturbations (e.g., Fermi-type dyad structure) in an acetylene monomer persist in corresponding complexes.[35] For example, the separate $(\nu_3/\nu_2 + \nu_4 + \nu_5)_I$ and $(\nu_3/\nu_2 + \nu_4 + \nu_5)_{II}$ dyad eigenstates of the C_2H_2 monomer are found to persist in weakly bound complexes such as $C_2H_2-CO_2$, C_2H_2-Ar, and C_2H_2-Ne[94] and also (probably) the dimer $(C_2H_2)_2$.[11] However, no such Fermi-type dyad structure is observed in more strongly bound H-bonded complexes of C_2H_2, such as C_2H_2-HF, C_2H_2-HCN, and C_2H_2-HX or C_2H_2-DX (X = Cl, Br, I).[93] Incidentally, we consider formation of van der Waals dimers most unlikely under the experimental conditions of our IR−UV DR experiments in which CIQCB effects have been observed ($T = 300$ K and *either* $P_{total} = 0.2$ Torr of pure C_2H_2 gas *or* $P_{total} = 1.1$ Torr of a 1:10 C_2H_2/Ar gas mixture).[42]

In this context, a relevant application of high-resolution optothermal rovibrational spectroscopy is the IR−IR double-resonance study of the $6\nu_3$, or $(0\ 0\ 6\ 0\ 0)^0$, Σ_g^+ vibrational overtone level in the $6\nu_{CH}$ manifold of C_2H_2 at ~18 400 cm^{-1}.[25] The IR-bright $6\nu_3$ Σ_g^+ $J = 2$ and $J = 4$ levels exhibit splittings that are attributed to local perturbations *via* couplings to the full density of vibrational states expected in in the $6\nu_{CH}$ manifold of C_2H_2.[25] However, there is no evidence of tunneling splittings that would indicate the mechanistically significant isomerization of C_2H_2 to vinylidene ($H_2C{=}C{:}$) that might be expected at such a high vibrational energy.[25,40,86g,87,97,98]

The above investigation[25] revisits our opening theme of significant advances in molecular physics that rely on innovative, high-performance instrumentation;[8] it exemplifies a variety of eigenstate-resolved IR spectroscopic studies of congested polyatomic-molecular rovibrational manifolds, performed with optothermal detection by Lehmann, Scoles, and co-workers.[22−26] In particular, we also note their measurements[23] of high-resolution optothermal rovibrational spectra for the ν_{CH}, $2\nu_{CH}$, and $3\nu_{CH}$ acetylene stretching bands of propyne (CH_3CCH) and for the $2\nu_{CH}$ band of trifluoropropyne (CF_3CCH); these provide interesting contrasts with the lighter, supposedly simpler (but apparently not much less complicated!) C_2H_2 molecule in its $4\nu_{CH}$ region, on which the present paper has focused.

Acknowledgment. Financial support from the Australian Research Council (ARC) is gratefully acknowledged, including the award of an ARC Postdoctoral Fellowship to A.P.M.

References and Notes

(1) (a) Gough, T. E.; Miller, R. E.; Scoles, G. *Appl. Phys. Lett.* **1977**, *30*, 338. (b) Gough, T. E.; Miller, R. E.; Scoles, G. *J. Mol. Spectrosc.* **1978**, *72*, 124. (c) Gough, T. E.; Miller, R. E.; Scoles, G. *J. Chem. Phys.* **1978**, *69*, 1588. (d) Gough, T. E.; Miller, R. E.; Scoles, G. *Faraday Discuss.* **1981**, *71*, 77. (e) Gough, T. E.; Miller, R. E.; Scoles, G. *J. Phys. Chem.* **1981**, *85*, 4041.

(2) Miller, R. E. In *Atomic and Molecular Beam Methods*; Scoles, G., Ed.; Oxford University Press: Oxford, U.K., 1992; Vol. 2, Chapter 4, p 192.

(3) Zen, M. In *Atomic and Molecular Beam Methods*; Scoles, G., Ed.; Oxford University Press: Oxford, U.K., 1988; Vol. 1, Chapter 10, p 254.

(4) (a) Cavallini, M.; Gallinaro, G.; Scoles, G. *Z. Naturforsch. A* **1967**, *22*, 413. (b) Cavallini, M.; Gallinaro, G.; Scoles, G. *Z. Naturforsch. A* **1967**, *24*, 1850. (c) Cavallini, M.; Meneghetti, G.; Scoles, G.; Yealland, M. *Rev. Sci. Instrum.* **1971**, *42*, 1759.

(5) Mollenauer, L. F.; Olson, D. H. *J. Appl. Phys.* **1975**, *46*, 3109.

(6) Boughton, C. V.; Miller, R. E.; Watts, R. O. *Aust. J. Phys.* **1982**, *35*, 611.

(7) Scoles, G. In *Atomic and Molecular Beam Methods*; Scoles, G., Ed.; Oxford University Press: Oxford, U.K., 1988; Vol. 1, Chapter 1, p 3.

(8) Srivastava, H. K.; Conjusteau, A.; Mabuchi, H.; Callegari, A.; Lehmann, K. K.; Scoles, G. *Rev. Sci. Instrum.* **2000**, *71*, 4032.

(9) Scoles, G. In *Abstracts of Papers, 220th ACS National Meeting (Washington, DC, 20−24 August 2000)*; American Chemical Society: Washington, DC, 2000; Paper ANYL-131.

(10) (a) Miller, R. E. *J. Phys. Chem.* **1986**, *90*, 3301. (b) Miller, R. E. *Science* **1988**, *240*, 447. (c) Miller, R. E. *Acc. Chem. Res.* **1990**, *23*, 10. (d) Bačić, Z.; Miller, R. E. *J. Phys. Chem.* **1996**, *100*, 12945.

(11) (a) Miller, R. E.; Vohralik, P. F.; Watts, R. O. *J. Chem. Phys.* **1984**, ***80***, 5453. (b) Fischer, G.; Miller, R. E.; Vohralik, P. F.; Watts, R. O. *J. Chem. Phys.* **1985**, *83*, 1471.

(12) Miller, R. E.; Vohralik, P. F. *J. Chem. Phys.* **1985**, *83*, 1609.

(13) (a) Bohac, E. J.; Wu, M.; Miller, R. E. *Phys. Rev. Lett.* **1993**, *71*, 54. (b) Wu, M.; Bemish, R. J.; Miller, R. E. *J. Chem. Phys.* **1994**, *101*, 9447. (c) Bemish, R. J.; Bohac, E. J.; Wu, M.; Miller, R. E. *J. Chem. Phys.* **1994**, *101*, 9457. (d) Bemish, R. J.; Wu, M.; Miller, R. E. *Faraday Discuss.* **1994**, *97*, 57.

(14) (a) Oudejans, L.; Miller, R. E. *J. Chem. Phys.* **1998**, *109*, 3474. (b) Oudejans, L.; Moore, D. T.; Miller, R. E. *J. Chem. Phys.* **1999**, *110*, 209 and 7109. (c) Oudejans, L.; Miller, R. E. *Annu. Rev. Phys. Chem.* **2001**, *52*, 607.

(15) (a) Boughton, C. V.; Miller, R. E.; Watts, R. O. *Mol. Phys.* **1985**, *56*, 363. (b) Boughton, C. V.; Miller, R. E.; Vohralik, P. F.; Watts, R. O. *Mol. Phys.* **1986**, *58*, 827. (c) Miller, R. E.; Vohralik, P. F.; Watts, R. O. *J. Chem. Phys.* **1986**, *85*, 3891.

(16) (a) Gough, T. E.; Orr, B. J.; Scoles, G. *J. Mol. Spectrosc.* **1983**, *99*, 143. (b) Gu, X. J.; Gough, T. E.; Isenor, N. R.; Scoles, G. *Phys. Rev. A* **1987**, *36*, 4722. (c) Gu, X. J.; Isenor, N. R.; Scoles, G. *Phys. Rev. A* **1989**, *39*, 413.

(17) Barnes, J. A.; Gough, T. E.; Stoer, M. *Chem. Phys. Lett.* **1995**, *237*, 437.

(18) (a) Barnes, J. A.; Gough, T. E.; Stoer, M. *Rev. Sci. Instrum.* **1999**, *70*, 3515. (b) Barnes, J. A.; Gough, T. E.; Stoer, M. *J. Chem. Phys.* **2001**, *114*, 4490.

(19) (a) Bemish, R. J.; Bohac, E. J.; Wu, M.; Miller, R. E. *J. Chem. Phys.* **1994**, *101*, 9457. (b) Bemish, R. J.; Wu, M.; Miller, R. E. *Faraday Discuss.* **1994**, *97*, 57.

(20) Oudejans, L.; Miller, R. E.; Hase, W. L. *Faraday Discuss.* **1995**, *102*, 323.

(21) Oudejans, L.; Olson, D.; Miller, R. E. *J. Chem. Phys.* **1996**, *105*, 8515. (b) Oudejans, L.; Miller, R. E. *Chem. Phys.* **1998**, **239**, 345 (1998). (c) Oudejans, L.; Miller, R. E. *J. Phys. Chem. A* **1999**, *103*, 4791. (d) Oudejans, L.; Miller, R. E. *J. Chem. Phys.* **2000**, *113*, 4581.

(22) (a) Lehmann, K. K.; Pate, B. H.; Scoles, G. *J. Chem. Soc., Faraday Trans.* **1990**, *86*, 2071. (b) Gambogi, J. E.; Becucci, M.; O'Brien, C. J.; Lehmann, K. K.; Scoles, G. *Ber. Bunsen-Ges. Phys. Chem.* **1995**, *99*, 548.

(23) (a) Kerstel, E. R. T.; Lehmann, K. K.; Pate, B. H.; Scoles, G. *J. Chem. Phys.* **1994**, *100*, 2588. (b) McIlroy, A.; Nesbitt, D. J.; Kerstel, E. R. T.; Lehmann, K. K.; Pate, B. H.; Scoles, G. *J. Chem. Phys.* **1994**, *100*, 2596. (c) Gambogi, J. E.; Kerstel, E. R. T.; Lehmann, K. K.; Pate, B. H.; Scoles, G. *J. Chem. Phys.* **1994**, *100*, 2612. (d) Gambogi, J. E.; Becucci, M.; O'Brien, C. J.; Lehmann, K. K.; Scoles, G. *Ber. Bunsen-Ges. Phys. Chem.* **1995**, *99*, 548.

(24) (a) Lehmann, K. K.; Scoles, G.; Pate, B. H. *Annu. Rev. Phys. Chem.* **1994**, *45*, 241. (b) Keske, J.; McWhorter, D. A.; Pate, B. H. *Int. Rev. Phys. Chem.* **2000**, *19*, 363. (c) Keske, J. C.; Pate, B. H. *Annu. Rev. Phys. Chem.* **2000**, *51*, 323.

(25) Srivastava, H. K.; Conjusteau, A.; Mabuchi, H.; Lehmann, K. K.; Scoles, G.; Silva, M. L.; Field, R. W. *J. Chem. Phys.* **2000**, *113*, 7376.

(26) (a) Callegari, A.; Merker, U.; Engels, P.; Srivastava, H. K.; Lehmann, K. K.; Scoles, G. *J. Chem. Phys.* **2000**, *113*, 10583. (b) Callegari, A.; Pearman, R.; Choi, S.; Engels, P.; Srivastava, H. K.; Gruebele, M.; Lehmann, K. K.; Scoles, G. *Mol. Phys.* **2003**, *101*, 551.

(27) (a) Rowntree, P. A.; Scoles, G.; Riz-Suárez, J. C. *J. Phys. Chem.* **1990**, *94*, 8511. (b) Robinson, G. N.; Camillone, N.; Rowntree, P. A.; Liu, G. Y.; Wang, J.; Scoles, G. *J. Chem. Phys.* **1992**, *96*, 9212.

(28) (a) Glebov, A.; Miller, R. E.; Toennies, J. P. *J. Chem. Phys.* **1997**, *106*, 6499. (b) Picaud, S.; Hoang, P. N. M.; Giradet, C.; Glebov, A.; Miller, R. E.; Toennies, J. P. *Phys Rev. B* **1998**, *57*, 10090.

(29) (a) Francisco, T. W.; Camillone, N.; Miller, R. E. *Phys. Rev. Lett.* **1996**, ***77***, 1402. (b) Wight, A. C.; Miller, R. E. *J. Chem. Phys.* **1998**, *109*, 8626. (c) Wight, A. C.; Penno, M.; Miller, R. E. *J. Chem. Phys.* **1999**, *111*, 8622.

(30) (a) Goyal, S.; Schutt, D. L.; Scoles, G. *Phys. Rev. Lett.* **1992**, *69*, 933. (b) Goyal, S.; Schutt, D. L.; Scoles, G. *J. Phys. Chem.* **1993**, *97*, 2236. (c) Goyal, S.; Schutt, D. L.; Scoles, G. *Acc. Chem. Res.* **1993**, *26*, 123.

(31) Toennies, J. P.; Vilesov, A. *Annu. Rev. Phys. Chem.* **1998**, *49*, 1.

(32) (a) Lehmann, K. K.; Scoles, G. *Science* **1998**, *279*, 2065. (b) Scoles, G.; Lehmann, K. K. *Science* **2000**, *287*, 2429.

(33) (a) Reinhard, I.; Callegari, C.; Conjusteau, A.; Lehmann, K. K.; Scoles, G. *Phys. Rev. Lett.* **1999**, *82*, 5036. (b) Callegari, C.; Conjusteau, A.; Reinhard, I.; Lehmann, K. K.; Scoles, G. *J. Chem. Phys.* **2000**, *113*, 10535. (c) Callegari, C.; Lehmann, K. K.; Schmied, R.; Scoles, G. *J. Chem. Phys.* **2001**, *115*, 10090.

(34) (a) Miller, R. E. *Faraday Discuss.* **2001**, *118*, 1. (b) Choi, M. Y.; Douberly, G. E.; Falconer, T. M.; Lewis, W. K.; Lindsay, C. M.; Merritt, J. M.; Stiles, P. L.; Miller, R. E. *Int. Rev. Phys. Chem.* **2006**, *25*, 15.

(35) Orr, B. J. *Int. Rev. Phys. Chem.* **2006**, *25*, 655.

(36) Herman, M.; Campargue, A.; El Idrissi, M. I.; Vander Auwera, J. *J. Phys. Chem. Ref. Data* **2003**, *32*, 921.

(37) Payne, M. A.; Milce, A. P.; Frost, M. J.; Orr, B. J. *Chem. Phys. Lett.* **1997**, *265*, 244.

(38) Payne, M. A.; Milce, A. P.; Frost, M. J.; Orr, B. J. *Chem. Phys. Lett.* **2000**, *324*, 48.

(39) Payne, M. A.; Milce, A. P.; Frost, M. J.; Orr, B. J. *J. Phys. Chem. A* **2003**, *107*, 10759.

(40) Payne, M. A.; Milce, A. P.; Frost, M. J.; Orr, B. J. *J. Phys. Chem. B* **2005**, *109*, 8332.

(41) Payne, M. A.; Milce, A. P.; Frost, M. J.; Orr, B. J. *Z. Phys. Chem.* **2005**, *219*, 601.

(42) Payne, M. A.; Milce, A. P.; Frost, M. J.; Orr, B. J. *J. Phys. Chem. B* **2006**, *110*, 3307.

(43) Milce, A. P.; Barth, H.-D.; Orr, B. J. *J. Chem. Phys.* **1994**, *100*, 2398.

(44) Milce, A. P.; Orr, B. J. *J. Chem. Phys.* **1996**, *104*, 6423.

(45) Milce, A. P.; Orr, B. J. *J. Chem. Phys.* **1997**, *106*, 3592.

(46) Milce, A. P.; Orr, B. J. *J. Chem. Phys.* **2000**, *112*, 9319.

(47) Frost, M. J.; Smith, I. W. M. *Chem. Phys. Lett.* **1992**, *191*, 574.

(48) Frost, M. J. *J. Chem. Phys.* **1993**, *98*, 8572.

(49) Frost, M. J.; Smith, I. W. M. *J. Phys. Chem.* **1995**, *99*, 1094.

(50) Henton, S.; Islam, M.; Smith, I. W. M. *Chem. Phys. Lett.* **1998**, *291*, 223.

(51) Henton, S.; Islam, M.; Smith, I. W. M. *J. Chem. Soc., Faraday Trans.* **1998**, *94*, (1998).

(52) Henton, S.; Islam, M.; Gatenby, S.; Smith, I. W. M. *J. Chem. Soc., Faraday Trans.* **1998**, *94*, 3219.

(53) Orr, B. J. *Chem. Phys.* **1995**, *190*, 261.

(54) Orr, B. J. In *Advances in Chemical Kinetics and Dynamics−Vibrational Energy Transfer Involving Large and Small Molecules*; Barker, J. R., Ed.; JAI Press: Greenwich, CN., 1995; Vol. 2A, p 21.

(55) Carrasquillo, M. E.; Utz, A. L.; Crim, F. F. *J. Chem. Phys.* **1988**, *88*, 5976.

(56) Utz, A. L.; Tobiason, J. D.; Carrasquillo, M. E.; Fritz, M. D.; Crim, F. F. *J. Chem. Phys.* **1992**, *97*, 389.

(57) Tobiason, J. D.; Utz, A. L.; Crim, F. F. *J. Chem. Phys.* **1992**, *97*, 7437.

(58) Utz, A. L.; Tobiason, J. D.; Carrasquillo, M. E.; Sanders, L. J.; Crim, F. F. *J. Chem. Phys.* **1993**, *98*, 2742.

(59) Tobiason, J. D.; Utz, A. L.; Crim, F. F. *J. Chem. Phys.* **1993**, *99*, 928.

(60) Tobiason, J. D.; Utz, A. L.; Sibert, E. L.; Crim, F. F. *J. Chem. Phys.* **1993**, *90*, 5762.

(61) Tobiason, J. D.; Utz, A. L.; Crim, F. F. *J. Chem. Phys.* **1994**, *101*, 1108.

(62) Tobiason, J. D.; Fritz, M. D.; Crim, F. F. *J. Chem. Phys.* **1994**, *101*, 9642.

(63) Utz, A. L.; Carrasquillo, M. E.; Tobiason, J. D.; Crim, F. F. *Chem. Phys.* **1995**, *190*, 311.

(64) Herman, M.; Liévin, J.; Vander Auwera, J.; Campargue, A. *Adv. Chem. Phys.* **1999**, *108*, 1.

(65) El Idrissi, M. I.; Liévin, J.; Campargue, A.; Herman, M. *J. Chem. Phys.* **1999**, *110*, 2074.

(66) Baxter, G. W.; Payne, M. A.; Austin, B. D. W.; Halloway, C. A.; Haub, J. G.; He, Y.; Milce, A. P.; Nibler, J. W.; Orr, B. J. *Appl. Phys. B* **2000**, *71*, 651.

(67) (a) Smith, B. C.; Winn, J. S. *J. Chem. Phys.* **1991**, *94*, 4120. (b) Zhan, X.; Halonen, L. *J. Mol. Spectrosc.* **1993**, *160*, 464. (c) Herregodts, F.; Hurtmans, D.; Vander Auwera, J.; Herman, M. *J. Chem. Phys.* **1999**, *111*, 7954. (d) Herregodts, F.; Hepp, M.; Hurtmans, D.; Vander Auwera, J.; Herman, M. *J. Chem. Phys.* **1999**, *111*, 7961.

(68) Hurtmans, D.; Kassi, S.; Depiesse, C.; Herman, M. *Mol. Phys.* **2002**, *100*, 3507.

(69) Payne, M.A. Ph.D. Thesis, Macquarie University, Sydney, Australia, 1999.

(70) Chadwick, B. L.; Orr, B. J. *J. Chem. Phys.* **1991**, *95*, 5476.

(71) Metsälä, M.; Yang, S.; Vaittinen, O.; Halonen, L. *J. Chem. Phys.* **2002**, *117*, 8686.
(72) (a) Gordon, R. G. *J. Chem. Phys.* **46**, 4399 (1967). (b) Steinfeld, J. I.; Houston, P. L. In *Laser and Coherence Spectroscopy*; Steinfeld, J. I., Ed.; Plenum Press: New York, 1978; Chapter 1, p 1.
(73) Bewick, C. P.; Haub, J. G.; Hynes, R. G.; Martins, J. F.; Orr, B. J. *J. Chem. Phys.* **88**, 6350 (1988).
(74) Bewick, C. P.; Orr, B. J. *J. Chem. Phys.* **1990**, *93*, 8634.
(75) Bewick, C. P.; Martins, J. F.; Orr, B. J. *J. Chem. Phys.* **1990**, *93*, 8643.
(76) Orr, B. J. *Int. Rev. Phys. Chem*. **1990**, *9*, 67.
(77) Bialkowski, S. E.; King, D. S.; Stephenson, J. C. *J. Chem. Phys.* **1979**, *72*, 1156.
(78) Brunner, T. A.; Pritchard, D. *Adv. Chem. Phys.* **1982**, *50*, 589.
(79) (a) Dopheide, R.; Gao, W. B.; Zacharias, *Chem. Phys. Lett.* **1991**, *182*, 21. (b) Dopheide, R.; Cronrath, W.; Zacharias, H. *J. Chem. Phys.* **1994**, *101*, 5804.
(80) (a) McCaffery, A. J.; Alwahabi, Z. T.; Osborne, M. A.; Williams, C. J. *J. Chem. Phys.* **1993**, *98*, 4586. (b) Osborne, M. A.; McCaffery, A. J. *J. Chem. Phys.* **1994**, *101*, 5604.
(81) Sitz, G. O.; Farrow, R. L. *J. Chem. Phys.* **1990**, *93*, 7883.
(82) Dopheide, R.; Cronrath, W.; Zacharias, H. *Chem. Phys. Lett.* **1994**, *222*, 191.
(83) Brown, J. M.; Hougen, J. T.; Huber, K.-P.; Johns, J. W. C.; Kopp, I.; Lefebvre-Brion, H.; Merer, A. J.; Ramsay, D. A.; Rostas, J.; Zare, R. N. *J. Mol. Spectrosc.* **1975**, *55*, 500.
(84) (a) Jacquemart, D.; Mandin, J.-Y.; Dana, V.; Claveau, C.; Vander Auwera, J.; Herman, M.; Rothman, L. S.; Regalia-Jarlot, L.; Barbe, A. *J. Quant. Spectrosc. Radiat. Transfer* **2003**, *82*, 363. (b) Perevalov, V. I.; Lyulin, O. M.; Jacquemart, D.; Claveau, C.; Teffo, J.-L.; Dana, V.; Mandin, J.-Y.; Valentin, A. *J. Mol. Spectrosc.* **2003**, *218*, 180. (c) Rothman, L. S.; Jacquemart, D.; Barbe, A.; Chris, Benner, D.; Birk, M.; Brown, L. R.; Carleer, M. R.; Chackerian, C., Jr.; Chance, K.; Coudert, L. H.; Dana, V.; Devi, V. M.; Flaud, J.-M.; Gamache, R. R.; Goldman, A.; Hartmann, J.-M.; Jucks, K. W.; Maki, A. G.; Mandin, J.-Y.; Massie, S. T.; Orphal, J.; Perrin, A.; Rinsland, C. P.; Smith, M. A. H.; Tennyson, J.; Tolchenov, R. N.; Toth, R. A.; Vander Auwera, J.; Varanasi, P.; Wagner, G. *J. Quant. Spectrosc. Radiat. Transfer* **2005**, *96*, 139.
(85) (a) Jonas, D. M.; Solina, S. A. B.; Rajaram, B.; Silbey, R. J.; Field, R. W.; Yamanouchi, K.; Tsuchiya, S. *J. Chem. Phys.* **1993**, *99*, 7350. (b) Nesbitt, D. J.; Field, R. W. *J. Phys. Chem.* **1996**, *100*, 12735. (c) Drucker, S.; O'Brien, J. P.; Patel, P.; Field, R. W. *J. Chem. Phys.* **1997**, *106*, 3423. (d) Moss, D. B.; Duan, Z.; Jacobson, M. P.; O'Brien, J. P.; Field, R. W. *J. Mol. Spectrosc.* **2000**, *199*, 265. (e) Silva, M.; Jongma, R.; Field, R. W.; Wodtke, A. M. *Annu. Rev. Phys. Chem.* **2001**, *52*, 811.
(86) (a) Solina, S. A. B.; O'Brien, J. P.; Field, R. W.; Polik, W. F. *Ber. Bunsen-Ges. Phys. Chem.* **1995**, *99*, 555. (b) Abboutti, Temsamani, M.; Herman, M.; Solina, S. A. B.; O'Brien, J. P.; Field, R. W. *J. Chem. Phys.* **1996**, *105*, 11357. (c) Solina, S. A. B.; O'Brien, J. P.; Field, R. W.; Polik, W. F. *J. Phys. Chem.* **1996**, *100*, 7797. (d) O'Brien, J. P.; Jacobson, M. P.; Sokol, J. J.; Coy, S. L.; Field, R. W. *J. Chem. Phys.* **1998**, *108*, 7100. (e) Jacobson, M. P.; O'Brien, J. P.; Silbey, R. J.; Field, R. W. *J. Chem. Phys.* **1998**, *109*, 121. (f) Jacobson, M. P.; O'Brien, J. P.; Field, R. W. *J. Chem. Phys.* **1998**, *109*, 3831. (g) Jacobson, M. P.; Field, R. W. *J. Phys. Chem. A* **2000**, *104*, 3073. (h) Hoshina, K.; Iwasaki, A.; Yamanouchi, K.; Jacobson, M. P; Field, R. W. *J. Chem. Phys.* **2001**, *114*, 7424. (i) Silva, M. L.; Jacobson, M. P.; Duan, Z.; Field, R. W. *J. Chem. Phys.* **2002**, *116*, 7939.
(87) Schork, R.; Köppel, J. M. *J. Chem. Phys.* **2001**, *115*, 7907.
(88) (a) Jungner, P.; Halonen, L. *J. Chem. Phys.* **1997**, *107*, 1680. (b) Saarinen, M.; Permogorov, D.; Halonen, L. *J. Chem. Phys.* **1999**, *110*, 1424.
(89) Metsälä, M.; Yang, S.; Vaittinen, O.; Halonen, L. *J. Chem. Phys.* **2002**, *117*, 8686.
(90) Sheng, X.; Ganot, Y.; Rosenwaks, S.; Bar, I. *J. Chem. Phys.* **2002**, *117*, 6511.
(91) Herregodts, F.; Hurtmans, D.; Vander Auwera, J.; Herman, M. *Chem. Phys. Lett.* **2000**, *316*, 460.
(92) Tobiason, J. D. Ph.D. Thesis; University of Wisconsin—Madison, Madison, WI, 1992.
(93) (a) Huang, Z. S.; Miller, R. E. *J. Chem. Phys.* **1987**, *86*, 6059. (b) Huang, Z. S.; Miller, R. E. *J. Chem. Phys.* **1989**, *90*, 1478. (c) Dayton, D. C.; Block, P. A.; Miller, R. E. *J. Phys. Chem.* **1991**, *95*, 2881.
(94) (a) Huang, Z. S.; Miller, R. E. *Chem. Phys.* **1989**, *132*, 185. (b) Bemish, R. J.; Block, P. A.; Pedersen, L. G.; Wang, Y.; Miller, R. E. *J. Chem. Phys.* **1993**, *99*, 8585. (c) Bemish, R. J.; Miller, R. E. *Chem. Phys. Lett.* **1997**, *281*, 272. (d) Bemish, R. J.; Oudejans, L.; Miller, R. E.; Moszynski, R.; Heijmen, T. G. A.; Korona, T.; Wormer, P. E. S.; van der Avoird, A. *J. Chem. Phys.* **1998**, *109*, 8968.
(95) (a) Block, P. A.; Jucks, K. W.; Pedersen, L. G.; Miller, R. E. *Chem. Phys.* **1989**, *139*, 15. (b) Block, P. A.; Marshall, M.; Pedersen, L. G.; Miller, R. E. *J. Chem. Phys.* **1992**, *96*, 7321. (c) Moore, D. T.; Oudejans, L.; Miller, R. E. *J. Chem. Phys.* **1999**, *110*, 197. (d) Hünig, L.; Oudejans, L.; Miller, R. E. *J. Mol. Spectrosc.* **2000**, *204*, 148.
(96) (a) Nauta, K.; Miller, R. E. *J. Chem. Phys.* **2001**, *115*, 8384. (b) Nauta, K.; Miller, R. E. *Chem. Phys. Lett.* **2001**, *346*, 129. (c) Nauta, K.; Miller, R. E. *Chem. Phys. Lett.* **2003**, *377*, 384. (d) Nauta, K.; Miller, R. E. *J. Phys. Chem. A* **2004**, *108*, 9908.
(97) Gallo, M. M.; Hamilton, T. P.; Schaefer, H. F. *J. Am. Chem. Soc.* **1990**, *112*, 8714.
(98) (a) Zou, S.; Bowman, J. M. *J. Chem. Phys.* **2002**, *116*, 6667. (b) Zou, S.; Bowman, J. M. *J. Chem. Phys.* **2002**, *117*, 5507. (c) Zou, S.; Bowman, J. M. *Chem. Phys. Lett.* **2002**, *368*, 421. (d) Zou, S.; Bowman, J. M.; Brown, A. *J. Chem. Phys.* **2003**, *118*, 10012. (e) Xu, D.; Guo, H.; Zou, S.; Bowman, J. M. *Chem. Phys. Lett.* **2003**, *377*, 582. (f) Loh, Z.-H.; Field, R. W. *J. Chem. Phys.* **2003**, *118*, 4037. (g) Yang, S.; Tyng, V.; Kellman, M. E. *J. Phys. Chem. A* **2003**, *107*, 8345. (h) Bittner, M.; Köppel, H. *Phys. Chem. Chem. Phys* **2003**, *5*, 4604. (i) Kozin, I. N.; Law, M. M.; Tennyson, J. M.; Hutson, J. M. *J. Chem. Phys.* **2005**, *122*, 064309. (j) Tremblay, J. C.; Carrington, T. *Can. J. Chem. Phys.* **2006**, *125*, 094311.